Theses and Dissertations   Theses and Dissertations

8-1-2013

Computational Design Optimization of Arc Welding Process for Reduced Distortion in Welded Structures

Mohammad Refatul Islam

Follow this and additional works at: https://scholarsjunction.msstate.edu/td

Computational design optimization of arc welding process for reduced distortion in

welded structures

By

Mohammad Refatul Islam

A Thesis
Submitted to the Faculty of
Mississippi State University
in Partial Fulfillment of the Requirements
for the Degree of Master of Science
in Computational Engineering
in the Bagley College of Engineering

Mississippi State, Mississippi

August 2013

Computational design optimization of arc welding process for reduced distortion in

welded structures

By

Mohammad Refatul Islam

Approved:

_____   _____
Keiichi Motoyama   Masoud Rais-Rohani
Research Professor   Professor
Aerospace Engineering   Aerospace Engineering
(Thesis Director)   (Committee Member)

_____   _____
Douglas J. Bammann   Roger L. King
Professor   Professor
Mechanical Engineering   Computational Engineering
(Committee Member)   (Graduate Coordinator)

_____
Jerome A. Gilbert
Interim Dean
Bagley College of Engineering

Name: Mohammad Refatul Islam

Date of Degree: August 17, 2013

Institution: Mississippi State University

Major Field: Computational Engineering

Major Professor: Keiichi Motoyama

Title of Study: Computational design optimization of arc welding process for reduced distortion in welded structures

Pages in Study: 102

Candidate for Degree of Master of Science

An effective approach to determine optimum welding process parameters is implementation of advanced computer aided engineering (CAE) tool that integrates efficient optimization techniques and numerical welding simulation. In this thesis, an automated computational methodology to determine optimum arc welding process parameters is proposed. It is a coupled Genetic Algorithms (GA) and Finite Element (FE) based optimization method where GA directly utilizes output responses of FE based welding simulations for iterative optimization. Effectiveness of the method has been demonstrated by predicting optimum parameters of a lap joint specimen of two thin steel plates and automotive structure of nonlinear welding path for minimum distortion. Three dimensional FE models have been developed to simulate the arc welding process and subsequently, the models have been used by GA as the evaluation model for optimization. The optimization results show that such a CAE based methodology can contribute to facilitate the product design and development.

DEDICATION

To my dear wife, my parents and only elder brother

iii

TABLE OF CONTENTS

LIST OF FIGURES

viii

CHAPTER I

INTRODUCTION

1.1 Background and Motivation

Arc welding is a major joining process used in every manufacturing industry large or small. Industries like automotive, aerospace and shipbuilding rely heavily on arc welding because of its efficiency, economy and dependability as a metal joining method. However, welding can introduce significant distortion in the final welded geometry, which causes loss of dimensional control, costly rework and production delays [1]. In automotive industry, it is a common practice today to use thin-sectioned, high-strength sheet metals to achieve weight reduction of car body structure. But the structures made of relatively thin components are the most vulnerable to distortion when subjected to welding. Despite tremendous development in welding technology over the years, weld induced distortion is still one of the major obstacles for cost-effective fabrication of lightweight structures.

Distortion in welded structures is largely influenced by the design parameters of the welding process. Better control of these welding variables will eliminate the conditions that promote distortion [2]. However, since welding is a multi-variables dependent process, it is often difficult or impossible to achieve the optimum set of these factors by traditional trial-and-error-based experimental methods. Hence, industrial

1

welding processes today require a robust process design tool to determine optimum set of process control parameters for reduction of weld induced distortion in structures.

In recent years, rapid growth in computer power and performance has made it possible to simulate real-world welding processes through computers. Efficient and well-established computer aided engineering (CAE) tools are available today which can predict many complex welding phenomena with good accuracy. In this context, integration of welding simulation tools and numerical optimization techniques can make it possible to find optimum parameters computationally with less time and cost. It is believed that such an integrated CAE approach will not only improve the manufacturing side of welding process but also improve the design side as well. Furthermore, CAE-based optimization can reduce fabrication cost considerablely by eliminating the need for expensive distortion corrections and providing greater design flexibility to investigate higher number of test cases for optimization by limited modifications of the simulation model. Therefore, in this research work, the implication of simulation-based design optimization approach to improve welding process design has been investigated.

1.2   Description of Arc Welding Process

Arc welding applies to a large and diversified group of welding processes that use an electric arc as the source of heat to melt and join metals [3]. Gas Metal Arc Welding (GMAW) is the most popular arc welding process that uses an electric arc established between the continuously fed electrode and the metals for melting and joining the metal parts as shown in Figure 1.1. The electric energy of the established arc produces sufficiently high temperature to melt the base and weld metals along with the filler wire into a pool of molten metal to weld the two metal parts together. As the electrode is

moved along the weld path, the molten weld pool solidifies in its wake. The method uses an inert gas to shield the electrode tip, arc and molten weld pool from the surrounding air and thereby provides desired arc characteristics. The filler wire (wire electrode) is fed continuously and automatically from a reel through the welding gun and a variable speed motor and motor control is used to maintain uniform wire feed rate. Wire diameters ranging from 0.6 mm to 6.5 mm are used in GMAW, the size depending on the thickness of the part being joined and the desired deposition rate. Both direct current (DC) and alternating current (AC) can be used. GMAW is widely used in manufacturing operations in automotive, aerospace and shipbuilding industries for welding a variety of ferrous and nonferrous metals. It provides several advantages over other welding methods, including stable arc property, smooth metal transfer, low spatter loss, good weld penetration and higher deposition rate.
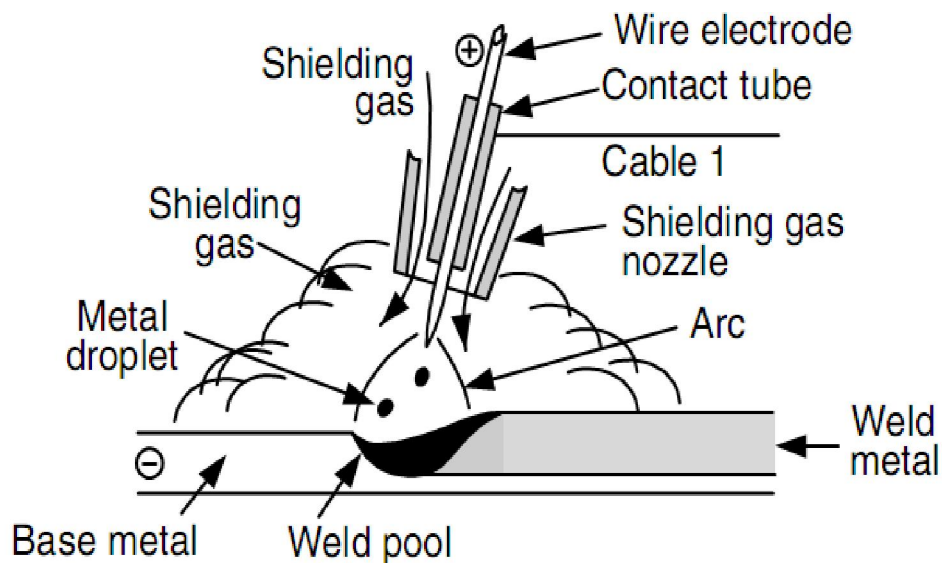
Figure 1.1   A schematic of Gas Metal Arc Welding Process [4]

1.3   Welding Distortion

Distortion in a weld results from the expansion and contraction of the weld metal and adjacent base metal during the heating and cooling cycle of the welding process [5]. Nonuniform heating and cooling cause complex thermal strains, and the stress resulting from the thermal strains produces internal forces causing shrinkage of the welded part. Depending on the shrinkage pattern and the shape of the structure welded, weld induced distortion can be classified into several types.

Masubuchi [6] classified welding distortion into six types as illustrated in Figure 1.2. Transverse shrinkage refers to the part shrinkage in transverse direction of weld line and longitudinal shrinkage occurs parallel to weld line. In rotational distortion, the parts start to open up as the welding torch moves ahead. Angular distortion is defined as change in angle of the plates in butt and fillet welds. Longitudinal bending is the bending with respect to the axis parallel to weld line. Buckling distortion is defined as elastic instability along the weld line.
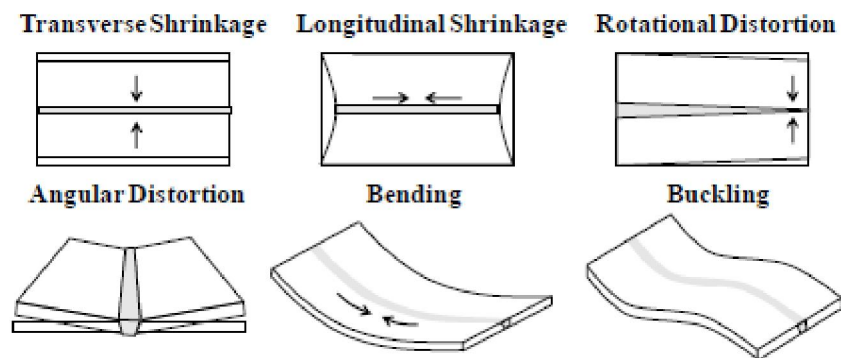
Figure 1.2   Different types of welding distortions [6]

1.4   Objective and Scope of this Research

The overall objective of this research effort is to establish an integrated CAE methodology for design and optimization of industrial welding processes to minimize weld induced distortion in the welded structures. The adopted approach is to employ a global optimization technique through Genetic Algorithms (GA) in conjunction with Finite Element Method (FEM) for welding process design. FEM has proven to be a versatile tool for predicting weld induced distortion and residual stresses of welding processes. Many researchers have investigated the generation of distortion during welding over the years using FEM. The advantage of the knowledge associated with the distortion phenomena can be augmented tremendously when FEM-based welding simulations are integrated with powerful global optimization technique like GA to obtain optimum process control parameters.

As there was no known integrated optimization/FEM system for welding process, a large portion of this work was devoted to such an integration. After performing a proof-of-concept optimization to verify the integrated system, the approach was successfully applied to a simple lap joint test case. After achieving promising results for the simple lap joint model, a complex automotive structure with nonlinear welding path was investigated for optimization. Due to the large amount of time to analyze each model, the computational model was simplified to perform the simulation within a reasonable timeframe. For both models, design of Experiments (DOE) methodology using Box-Behnken design combined with Response Surface Methodology (RSM) were employed to enhance the computational efficiency.

5

The methodology used in this research can be divided into three stages. The first stage consists of finite element (FE) modeling and welding simulation of both simple lap joint model and complex automotive structure model. For both cases, three-dimensional finite element models were developed and the necessary correlations were implemented to make the simulation models as accurate as possible for use in design optimization. Simulation prediction of the lap joint model was also validated by experimental results. During this stage, welding parameters that will be used as design variables in optimization were determined through analysis of parametric effect on welding simulation. The second stage is devoted to the development of a coupled GA and FE optimization system where GA directly utilizes output responses of FE-based welding simulation for optimization. The system is based on four computer programs: a process simulation program, an optimization program, a simulation input generation program and a simulation output analysis program. The four programs are integrated in a closed loop to establish an automatic and iterative optimization process as shown in Figure 1.3.
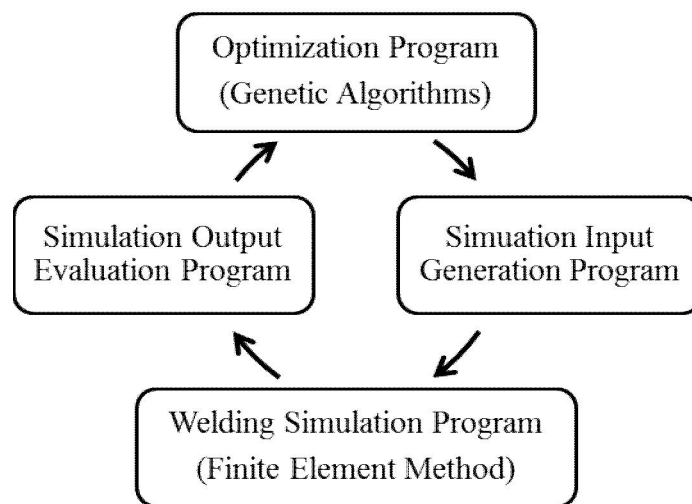
Figure 1.3   A general framework of computational optimization system

6

In third stage, the developed direct optimization system is used for simple lap joint model optimization. After initial trial optimization, consideration of the significant computational time and expense involved in the direct optimization process led to the use of DOE for design space exploration. A response surface model was created from the results of the DOE study. The developed optimization system was subsequently modified to conduct optimization using the RSM for objective function calculation instead of the simulation model. The results of all optimization efforts are presented later in Chapter V.

1.5   Organization of Thesis

This thesis is divided into six chapters. Chapter I provides a brief introduction to the background, motivation and overall methodology of the thesis. The next chapter mechanics of welding, welding simulations, weld induced distortions and simulation-based welding process optimization. Chapter III presents the details of the welding simulation approach taken in this research. First, a brief description of the simulation tool utilized is given, followed by a discussion of the FE modeling of the welding process. In Chapter IV, GA-based welding process optimization is presented at first. Next, details of the integration of GA and FEM is presented. Chapter V presents the findings of this study and the related discussions. Chapter VI summarizes the work performed in this research, and presents conclusions and recommendations for future research.

CHAPTER II

LITERATURE REVIEW

2.1   Finite Element Modeling and Simulation of Welding

2.1.1   Introduction

Welding is a complex thermomechanical process, which involves several stringent phenomena such as nonlinear heat flow, complex weld pool physics and nonlinear material behavior at elevated temperature. Therefore, computational modeling of welding process requires substantial expertise. Convergence of welding simulation is also often difficult because of the material behavior at elevated temperatures. Moreover, welding simulation requires quality meshing with sufficient mesh density along the welds and the heat-affected zone. This requires both time and expertise in FE mesh generation and usually results in a large number of degrees of freedom (DOF) in the model [7]. However, FEM is still the most popular and powerful tool used in simulating the thermomechanical behavior of a structure during welding [8].

Ueda and Yamakawa[9] and Hibbit and Marcal [10] are among the pioneers who successfully applied FEM for simulation of welding during the late 1970s. Ueda and Yamakawa [9] used FEM to analyze thermal transient stresses induced in butt welds with consideration of temperature dependent material properties. Hibbit and Marcal [10] treated the welding process as a thermo-mechanical problem and derived FE formulation from uncoupled thermal and mechanical energy balances. In 1974, Marcal [10] stated that

8

"welding is perhaps the most non-linear problem encountered in structural mechanics" and Goldak et at. [8] suggested this fact has discouraged many researchers from entering this research area. Hibbit and Marcal, then Ph.D. students, later established one software company each, developing two of the world's most popular nonlinear FE programs namely ABAQUS and MARC. These two computer software are the most frequently used solvers in welding simulation. Over the last three decades, a lot of research efforts have been made in the welding simulation domain and consequently, computational modeling of welding process has reached a mature and feasible stage in recent years. Lindgren [11] has explained the evolution of welding simulation through the increase in the size of the computational models as shown in Figure 2.1. To review all the works related to the welding simulation domain is beyond the scope of this work. The most significant and relevant contributions to the development of different aspects of welding process modeling have been discussed in later sections.
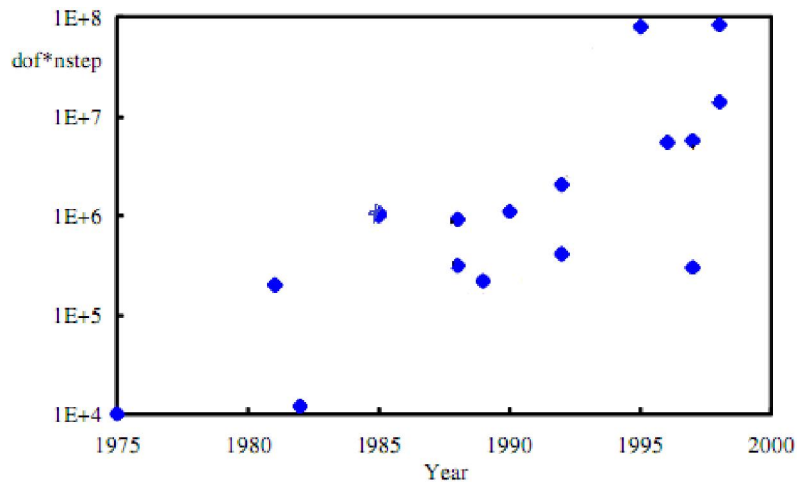
Figure 2.1   Size of computational models of welding measured by degree of freedom multiplied by number of time steps versus year of publication of work [11]

9

2.1.2   Evolution of FE Modeling Approach

Most of the earlier studies in the FEM-based welding simulation domain were conducted with two-dimensional (2D) models [12-14]. This is primarily because they give useful and sufficiently accurate results without the requirement of large computing power of three-dimensional models. In 2D models, the analysis is restricted to a plane perpendicular to the welding direction as shown in Figure 2.2. The out-of-plane behavior is treated as plane stress, plane strain, generalized plane strain or axisymmetric condition. In plane-stress condition, out-of-plane stress is assumed zero whereas out-of-plane strain is assumed zero in plane-strain condition. Both longitudinal heat flow and displacements are ignored under plane-strain condition. A constant strain is often assumed normal to the analysis plane that is known as generalized plane strain to compensate the error associated with high longitudinal restraint of plane-strain condition [15].

Analysed cross-section
Plane deformation or
plane strain model

a)

Analysed cross-section
Axisymmetric model

b)

Analysed plane
Plane stress model

c)
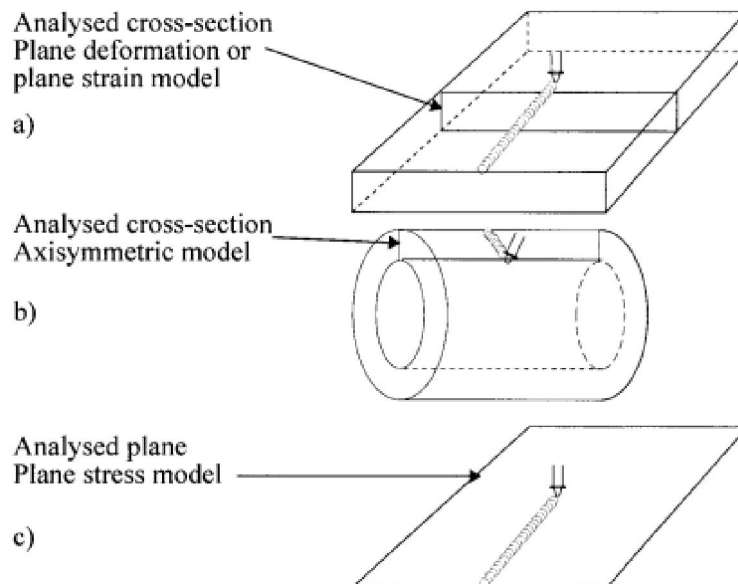
Figure 2.2   Two-dimensional models of welding [12]

2D models are accurate and suitable for residual stress predictions since residual stress distribution is more or less uniform along the welding direction. Rybicki et al. [16] implemented 2D axisymmetric computational models to predict transient temperature distributions, residual stresses, and residual deflections for girth-butt welds. Brickstad and Josefon [17] studied residual stress fields during multi-pass butt-welds using 8-noded biquadratic axisymmetric elements and conducted sensitivity analysis with respect to the variation in heat input.

Although 2D models are very useful in estimating residual stresses, effect of two-dimensional constraint on deformation and strain prediction is larger than that estimated [12]. 2D analysis may not be accurate for distortion prediction in presence of out-of-plane distortion induced by tack welding and fixturing [18]. However, considering the large computational time, many researchers implemented different techniques to find a trade-off between 2D and 3D models. Fujita et al. [19] combined plane-stress models to simulate the welding of a stiffener on a plate. Rybicki and Stonesifer [20] added stiffnesses orthogonal to a two-dimensional model of welding in order to include three-dimensional effects. These stiffnesses were obtained from a three-dimensional model of the structure. Michaleris and Debiccari [21, 22] proposed an uncoupled finite element analysis (FEA) technique for predicting welding-induced buckling distortion that combines two-dimensional welding simulations with three-dimensional structural analysis.

All stress and strain components in all three directions are included in three-dimensional solid models. Until the late 1990s, very few research studies were performed using full 3D models. Tekriwal and Mazumdar [23] simulated thermal cycle of a weld

joint using a three-dimensional model and compared simulation predicted heat-affected zone and the melt-pool zone with experimental observations. Karlsson and Josefson [24] implemented full 3D model with no assumption of axisymmetry to investigate residual compressive hoop stresses and circumferential stress variations for a single pass grove weld in a cylinder. Mahin, et al. [25] successfully conducted three-dimensional thermal and stress/strain simulations of welding process on plates and achieved good quantitative agreements between predicted and experimental results on temperature, displacement and stresses. Goldak et al. [26] examined the three-dimensional temperature, stress and strain fields associated with the butt joint welding of a bar, and subsequently considered additional geometries. Ueda et al. [27] simulated the multi-pass welding of plates and correlated their results with experimentally measured three-dimensional residual stress states. In recent years, three-dimensional welding simulations have been predominantly used to investigate thermomechanical behavior of welded structures.

2.1.3   Heat Source Modeling

The temperature history of welded components has a significant influence on residual stresses and distortion. All the FE simulations consider only the thermomechanical phenomena in the weld and incorporate all the physics of the welding process into empirical heat input model [28]. In FE simulation, the heat input is represented by either a prescribed heat flux or temperature. The first one is the most commonly used approach.

The most fundamental analytical method of predicting transient temperature field during welding is Rosenthal's solution [29] for traveling heat source. However, this solution considers instant point heat source, line heat source or surface heat source, which

are accurate enough to predict the temperature field at a distance far from the heat source, but its temperature prediction accuracy in the vicinity of the heat source is very poor [30]. Many researchers have tried to compensate for the limitations of Rosenthal's solution by implementing Gaussian distribution heat source. Pavelic et al. [31] suggested a heat source modeled with a Gaussian distribution of flux deposited on the surface of the workpiece. With this model, the concentration of the heat source can be varied by changing a parameter called the concentration coefficient. Friedmen, et al. [32] developed a variation of Pavelic's model that is expressed in coordinates that move with the heat source. Andersson [33] used surface heat input and an impulse equation for the heat contributed by the addition of filler. Usually, some kind of ramp with linearly increasing heat input for the approaching arc and constant heat input when the elements are melted and linearly decreasing heat input when the arc is leaving the element are used. Although these Gaussian heat sources are significant improvements over Rosenthal's basic model, they are still limited by the shortcoming of the 2D heat source itself without the effect of penetration [30].

Goldak, et al. [34] first proposed the nonaxisymmetrical three-dimensional heat source model which can treat both shallow and deep penetrations. They combined two ellipsoidal heat sources (as shown in Figure 2.1) to overcome the limitation of single ellipsoidal source associated with temperature gradient.
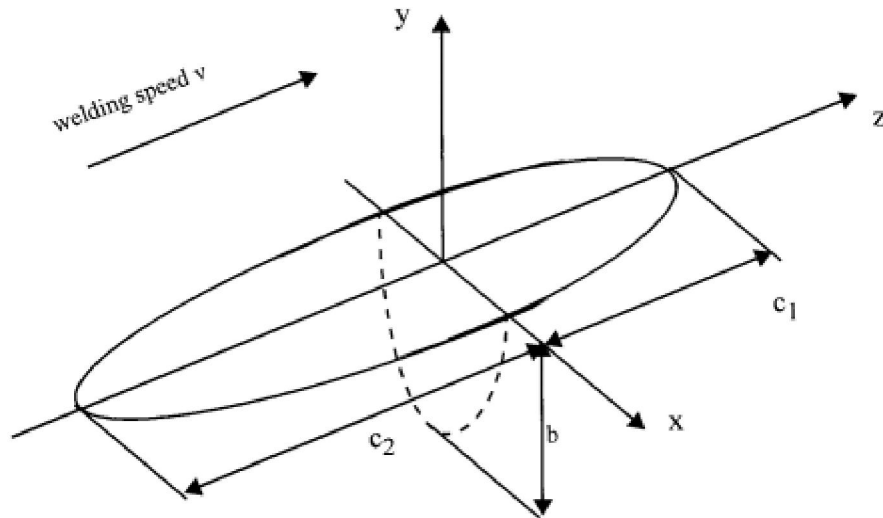
Figure 2.3   Geometry of double ellipsoidal heat source [12]

They implemented the heat source into FE modeling to calculate the temperature field of a bead-on-plate. The results showed that the double ellipsoid model, which spreads the thermal load throughout the weld pool, is more accurate than 2D Gaussian models where the thermal load is applied only to the surface of the weld [34]. The proposed three-dimensional 'double ellipsoid' configuration of heat source model is still the most popular and useful form of heat source model used in FE modeling of arc welding. The later heat source models, which included liquid weld pool and fluid flow phenomena, have been reviewed by Akhlagi and Goldak [8]. Additional useful information can be found in the book by Radaj [35].

2.1.4   FE Approach for Weld Distortion Simulation

As discussed in the previous chapter, weld induced distortion is still one of the most common problems in welding industry as it degrades dimensional tolerance and stability of finished products. Several researchers have attempted to understand distortion

14

phenomena using different predictive methodology, parametric experiments or empirical formulations since 1930 [36]. For three decades, FEM has been the most frequently adopted tool to predict weld-induced distortion.

The initial welding simulations [12-15] were highly simplified based on two-dimensional approach and plane strain condition. The results gave indications of the welding residual stresses evolved in quasi-static, plane strain situations, but did not give a picture of the total out-of-plane deformations [21-22]. Brown and Song [18] used both 2D and 3D models to investigate fixturing impact on large structures and concluded that full 3D models are essential in predicting welding distortion. Daniewicz [37] used hybrid (experimental and numerical) approach to predict weld distortions of large offshore structures. Murakawa et al. [38] and Luo et al. [39] proposed elastic FEA procedure to estimate welding distortion and residual stress based on inherent strain method. Michaleris et al. [21, 22] used two step numerical analysis approach that combines two-dimensional welding simulation with structural analysis for predicting buckling distortion. The residual stresses derived by two-dimensional welding simulation are used as loading in structural analysis. Two-dimensional welding simulation contributes substantially to reduce the computation time of entire analysis. The methodology was successfully applied for stiffened panel structures (as shown in Figure 2.2) with a particular emphasis on welding-induced buckling instabilities. Hinrichsen [40] also performed two-step analysis on single-pass fillet welds. Firstly, a thermo-elasto-plastic, two-dimensional model establishes the transverse shrinkage and in the second stage, the longitudinal shrinkage is found from a three-dimensional, shell element model, whereby

15

the whole length of the plate is assumed to be heated simultaneously along the weld

seam—similar to a plane deformation analysis.
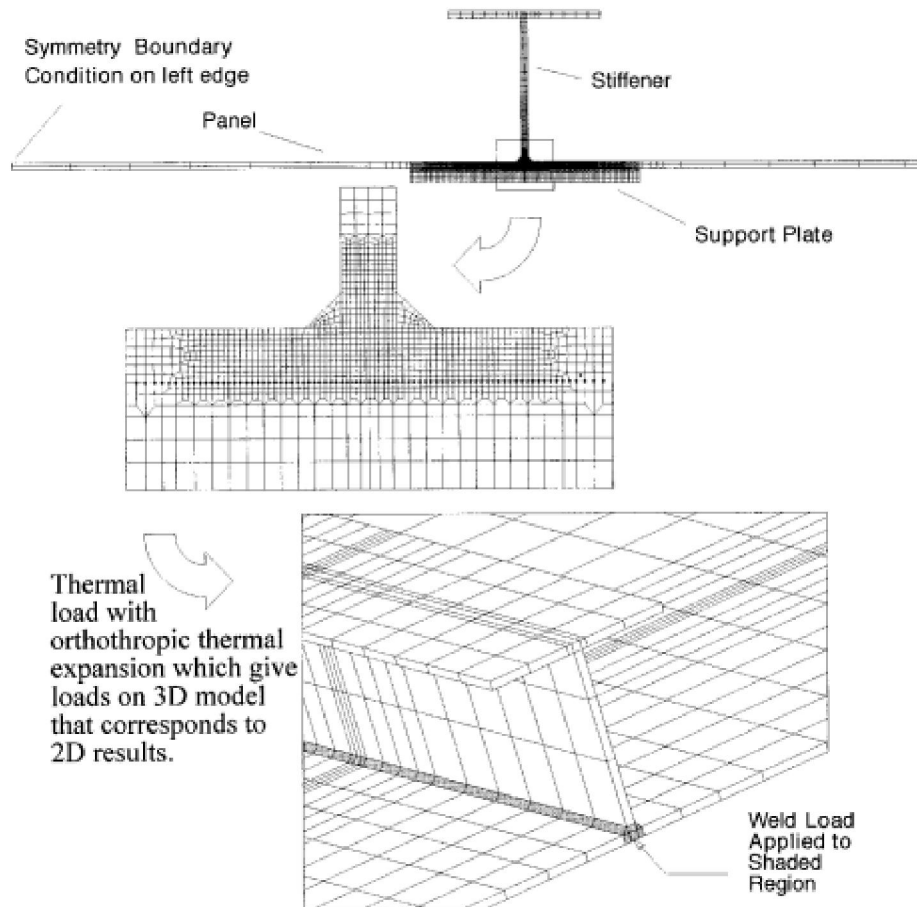
Figure 2.4   2D welding simulation model and 3D structural model [21,22]

Tsai et al. [2] has investigated distortion mechanism and the effect of welding

sequence on panel distortion using FEM based on joint rigidity method. Teng et al. [41]

performed thermo-elasto-plastic analysis using FEM to evaluate residual stress and

angular distortion in T-joint fillet welds and analyzed the effect of flange thickness,

welding penetration depth and restraint condition on angular distortion. Jung and Tsai

16

[42] developed a plasticity-based distortion analysis and applied it to investigate the relationship between cumulative plastic strains and angular distortion in a fillet welded T-joint. Camilleri et al. [43] proposed a method to improve the computational efficiency of generic FEM-based distortion prediction technique; they modified the full transient thermo-elasto-plastic analysis into an uncoupled thermal, elasto-plastic and structural treatment. A two-dimensional cross-section thermal model was used to establish thermal transients. The maximum temperatures, experienced at each node during the welding cycle, were then used to link the thermal welding strains to the elasto-plastic and structural response of the welded structures. Deng et al. [44, 45] have also conducted substantial research on predicting welding distortion of both thin and large structures. They have effectively used thermal elastic-plastic FEA to predict welding distortion in small or medium welded structures. However, the authors concluded this method is inapplicable to simulate the welding distortion for large welded structures because of the large amount of computational time [46]. They proposed an elastic FEM to predict welding distortion in large structures considering both local shrinkage and gap [47]. Murakawa et al. [48] extended the application of inherent strain theory and interface element formulation to compute distortion in thin plate structures.

2.2   Computational Optimization of Welding Process

Optimization of welding process to minimize weld-induced distortion in final structure has been an active research area for several decades. Two optimization approaches (i.e., experimental and computational) can be implemented to determine the optimum welding conditions. The first approach, where actual welding experiments are used, still dominates the published literature. An extensive review of experimental

17

optimization of welding process can be found in refs. [49 and50]. In experimental

optimization, DOE, Taguchi method, Evolutionary Algorithms and Artificial Neural

Networks are the most frequently used methods. For distortion control, many weld design

optimization procedures such as prestraining, weld sequencing and precambering were

developed by experiment and experience. However, with the advent of computational

weld models, which are quite accurate, new and creative distortion control methods are

emerging because the scenarios can be evaluated on the computer [51].

In computational optimization, numerical methods or models are used to replace

the expensive experimental works with computational evaluations. As such, optimization

work can be carried out using computers rather than real experiments. Computational

optimization approach is a well-established method for structural sizing, shape and

topology optimization in automotive and aerospace industry [52]. In welding industry,

this approach is yet to be adopted in full scale. According to Asadi and Goldak [53],

optimization of welding and welded structures is much less mature. Very few research

works have been conducted in the domain of welding optimization via welding

simulation.

Michaleris et al. [54] performed an optimization of a one-pass weld with respect

to manufacturing and service life aspects. Later [55] this was also done to determine

thermal tensioning, which minimizes residual stresses. Sensitivity analysis was

implemented to reduce the number of analyses in the minimization procedure. The inputs

are the chosen design variables, such as the welding procedure. The output can be

residual stresses or deformations, for example. More recently, Song et al. [56] have also

implemented similar sensitivity analysis to optimize quasi-static weakly coupled thermo-

elasto-plastic process for side heater design. The residual longitudinal compressive stress was chosen as objective function. The design variables were the side heat source, transverse position of the side heater and the distance between the side heater and first welding torch. The optimization was performed using BFGS line search method in the DOT package and FEA and sensitivity analysis were performed using in-house SMP FORTRAN 90 code.

Kadivar et al. [57] linked GA method with a thermomechanical model to determine optimum welding sequence of a circular specimen for minimization of distortion. A transient two-dimensional FE model was used to compute thermal history and a thermoelastic-viscoplastic FE model was used for mechanical analysis. In the optimization problem, the circular weld line was divided into eight parts and the order of welding for these parts and the direction of welding for each part were considered as design variables. Based on the optimization results, the authors concluded that distortion in welded structure can be greatly reduced by choosing optimum welding sequence.

Voutchkov et al. [58] and Goldak et al. [59] have also investigated weld sequence optimization for distortion minimization as combinatorial optimization problem, but they used surrogate models to replace the computation intensive FE models. Voutchkov et al. [66] applied the surrogate model to optimize the weld sequence for a tail bearing housing that mounts the engine to the body of the aircraft. The original weld path is divided into six sub-welds and each sub-weld can be done in two directions. A DOE table of 27 design points or weld sequences out of 46,080 possible combinations was chosen to construct the surrogate model. They showed the solution of the surrogate model was very accurate by comparing the surrogate solution with the FEM solution. Goldak et al. [59]

have also implemented similar surrogate modeling approach to minimize the distortion in a girth weld of a pipe.

In spite of the potential of computational optimization approach, few research works have been conducted in computational optimization welding process. Goldak and Asadi [60] have addressed this promising integration aspect and discussed in details the significance of computational optimization for improvement of welding process design. According to the authors, Computational Weld Mechanics (CWM) is not well integrated with optimization software. To achieve the ultimate goal of CWM, it must be integrated with computational optimization.

CHAPTER III

WELDING SIMULATION TECHNOLOGY

3.1 Governing Equations of Welding Thermomechanics

Computational modeling of welding is an inherent multiphysics problem. It involves several coupled phenomena such as complex weld pool physics, nonlinear heat flow, nonlinear material behavior at elevated temperature, generation of thermal stresses and mechanical deformations, etc. Lindgren [12-15] has provided an extensive review on different interactions present in the welding process. However, the mainstream approach in computational welding mechanics (CWM) is to use weakly coupled models where the physics in the weld is replaced by a heat input model [11]. Most analyses of CWM also implement a simplified coupling scheme as shown in Figure 3.1.
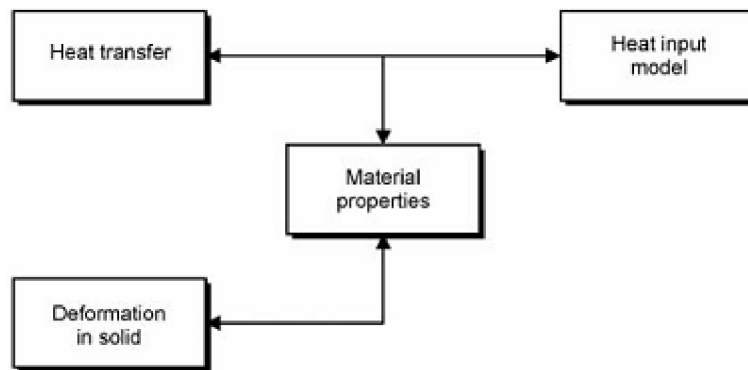
Figure 3.1   Simplified coupling scheme adopted in classical CWM [11]

The conservation of energy is the fundamental principle in thermal analysis of welding [8]. Therefore, during thermal analysis, stress, strain and displacement are ignored and only energy is considered. The energy balance between change in stored energy and heat flux [11,61, 62] is given by

$$\rho\dot{H} = \dot{Q} - \nabla.$$
(3.1)

where ρ is the density, $\dot{H}$ is the volumetric enthalpy or heat content, $\dot{Q}$ is the heat input per unit volume and **q** is the heat flux vector and $\nabla = (-, \frac{}{\partial y}, \frac{}{z})$ is the spatial gradient operator. The heat flux vector is defined by Fourier's law for isotropic materials as follows-

$$= -\mathbf{k}\nabla T$$
(3.2)

where k is the thermal conductivity matrix of material And ∇T is the temperature gradient. The enthalpy is related to the temperature by

$$H(T) = \int_{T_{ref}}^{T} cdT$$
(3.3)

The relations give the classical heat conduction equation which is as follows

$$\rho c \dot{T} = \dot{Q} - \nabla.(\mathbf{k}\nabla T)$$
(3.4)

where $\dot{T} = \frac{T}{t}$ with t is time parameter. To solve this differential equation, boundary conditions must be incorporated. The boundary conditions may be prescribed temperature or prescribed heat flux. By including convective, contact and radiation heat losses, the flux equation is written as

22

$$q_n = -\lambda \nabla \text{T}.\,\mathbf{n} = h(\text{T} - \text{T}_\infty) + \epsilon\sigma(\text{T}^4 - \text{T}_\infty^4) + a(\text{T} - \text{T}_{\text{contact}}) \qquad (3.5)$$

where the first term is convection heat loss and h is the convective heat transfer coefficient. The second term is emissive heat loss and ϵ is the emissivity factor. The third term is the contact heat loss and α is the contact heat transfer coefficient. In FEA, these boundary conditions are applied to the model by specifying the values of the heat transfer coefficients and the surrounding temperatures at the elements and nodes, respectively. The heat conduction equation, together with these boundary conditions define the basic thermal problem that needs to be solved by FEM during welding simulation.

In mechanical analysis, the basic equations are the equilibrium equations, constitutive stress-strain relations and geometric compatibility equations. A good flowchart of the complete FE formulation for thermal elasto-plastic model has been given by Teng [41] as shown in Figure 3.2.
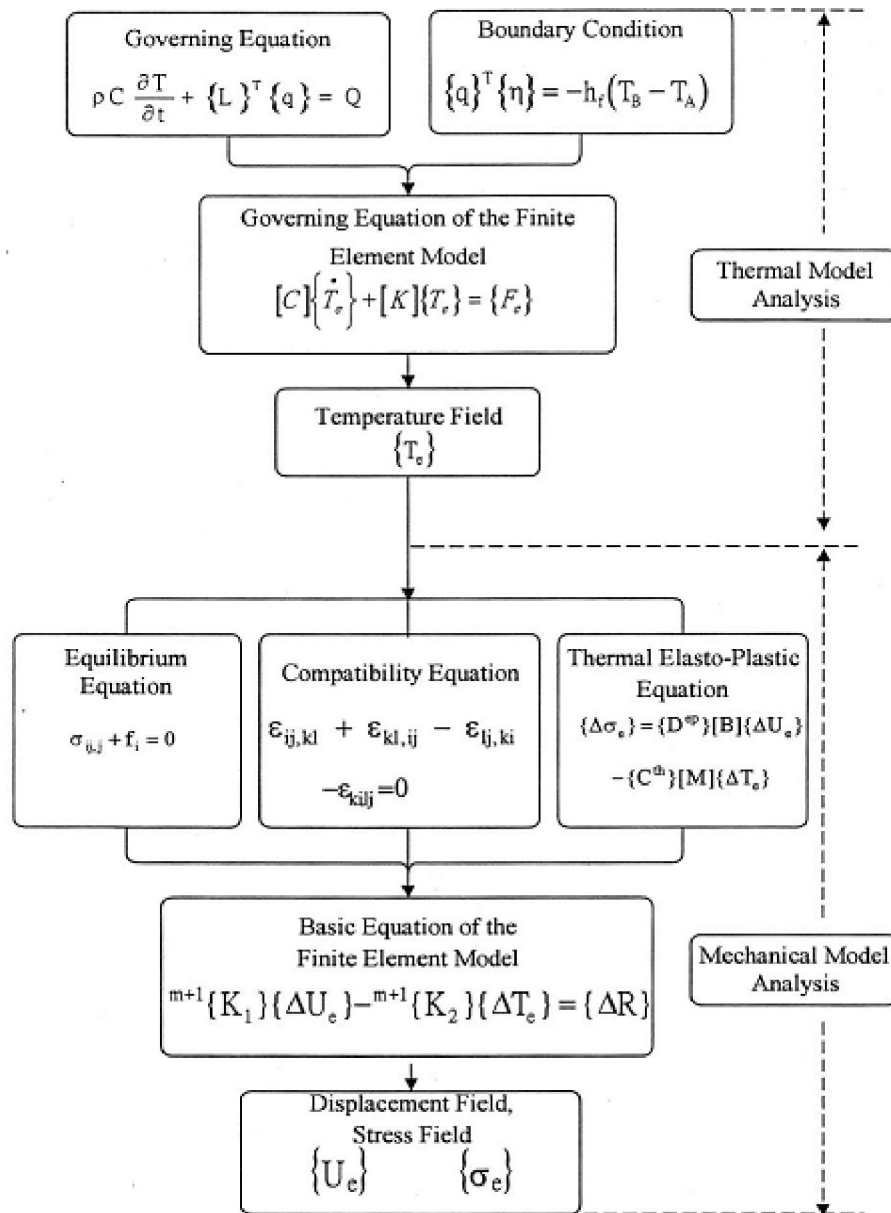
Figure 3.2   Flow diagram of finite element analysis procedure for welding [49]

3.2   Welding Simulation Tool

The welding simulation tool chosen for this research work is simufact.welding©, which is a Pre- and Postprocessor-GUI for FE welding process analysis [63]. There are several fundamental reasons for the selection of this FEM package, foremost among

which are its ability to simulate complex welding process model with multiple welding robots working at the same time or different times, flexibility to define or modify welding parameters, paths, directions and simple automatic batch running option useful for simulation-based design optimization.

Simufact.welding provides a user-friendly interface for configuring process modeling properties, solver settings, welding robot settings, heat source parameters and geometric boundary conditions. Simufact.welding supports two types of FE solvers: IFM WeldSim and MSC Marc. Both are capable of coupled thermomechanical analysis taking into account complex heat generation, nonlinear heat flow and temperature dependent material behavior. We conducted FEA using MSC Marc solver. For heat source modeling, Simufact.welding has two options: Goldak's double-ellipsoid source model and the volume- and area-distributed laser source. We implemented double ellipsoid source model because of its wide acceptance as efficient heat source model for arc welding. Simufact.welding requires each boundary condition to be assigned to a geometry. It provides three different options to model FE boundary conditions: bearing, fixing and clamping. A bearing represents a boundary condition which restraints a geometry in contact to move towards it. The fixing type boundary condition restraints all three transitional degrees of freedom and a clamping tool always acts in the normal direction of the contact area. The restraint motion directions of all three types of boundary conditions are shown in Figure 3.3.

25
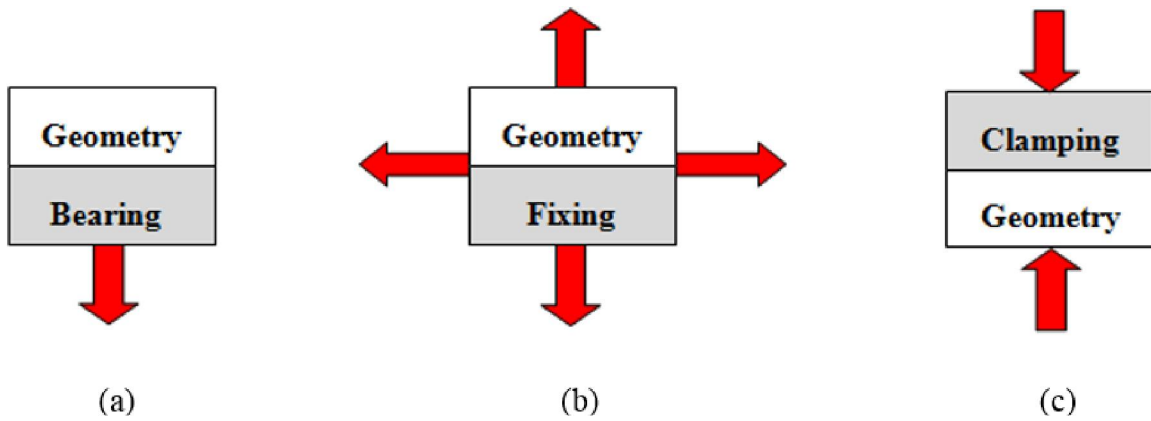
Figure 3.3   Constrained motion directions of three types of boundary conditions-
(a) bearing, (b) fixing and (c) clamping

3.3   Finite Element Modeling

3.3.1   Test Problems

We considered two different welding conditions to demonstrate the implementation of computational optimization system. The first model is a single pass welded lap-joint specimen. The plate dimensions are 170 x 35 x 3.2 mm and the weld length is 70 mm at the approximate middle section of the plates as shown in Figure 3.4. We conducted welding experiments in order to validate FE model of the lap-joint specimen. The experiments are discussed in the Appendix A. After successfully modeling, validating and optimizing the first model, we approached an automotive suspension part called lower arm with nonlinear welding path and sufficiently long weld length of 160 mm. The lower-arm model is shown in Figure 3.5.

3.3.2   Geometry Modeling

A full three-dimensional FE model of the lap-joint specimen was developed and the necessary correlations were implemented to make the model as accurate as possible.

26

The analysis was initiated by generating the model geometries in a suitable CAD system and then the geometries were meshed precisely. The entire FE model of the lap-joint specimen consists of three geometries: two to represent the base plates and one for weld bead as shown in Figure 3.4.
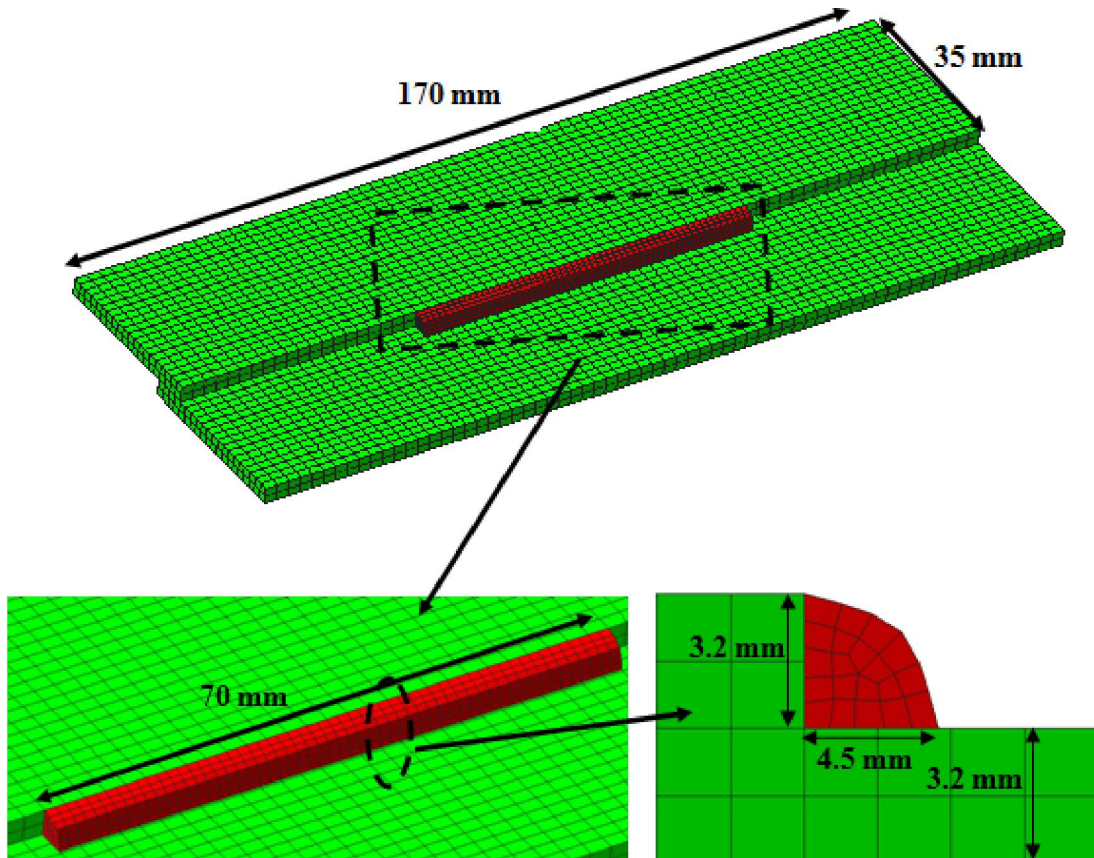
Figure 3.4   FE model of the lap-joint specimen and zoomed views of weld bead

The CAD model of the lower-arm specimen was provided by the manufacturing company F.tech R&D North America Inc. The lower-arm FE model consists of three geometries: two to represent the curvilinear parts to be joined and one for weld bead as

shown in Figure 3.5. However, the weld bead is subdivided into three sub-welds as shown in the zoomed views of the fillet element in Figure 3.5.
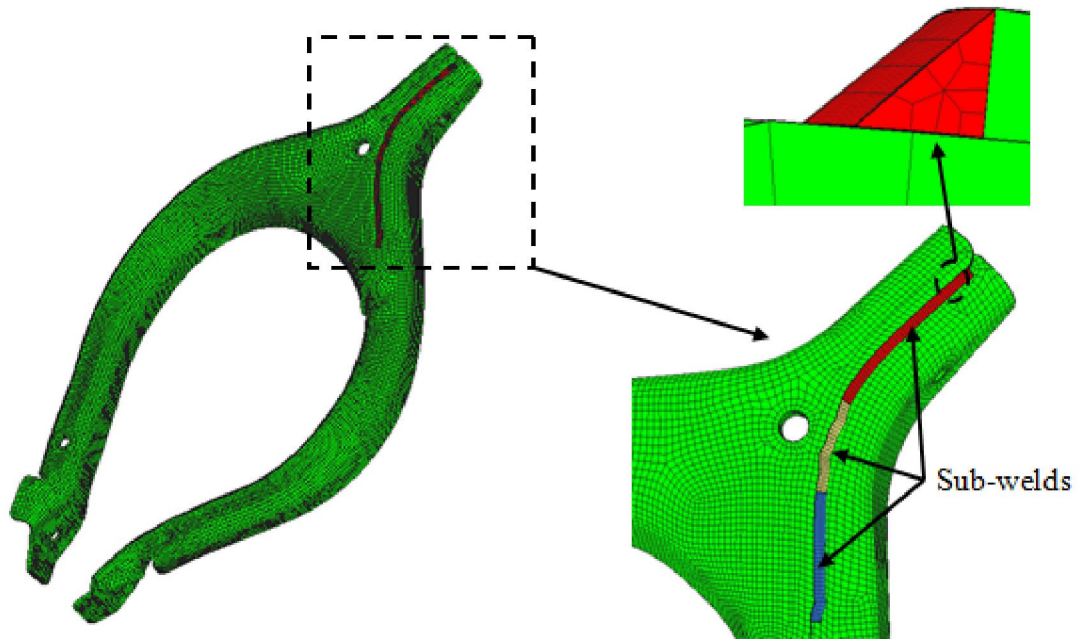
Figure 3.5   FE model of the lower arm specimen and zoomed view of weld bead

The lap-joint FE model contains 6,840 eight-node hexagonal elements and 10,347 nodes. As shown in the Figure 3.4, a uniform mesh of 1.75x1.25x1.6 mm is used for both base plates. For the fillet element, a one-level denser mesh is used and the weld bead element size along the weld path is 0.625 mm. To reduce computational time and achieve dense mesh in the weld zone, adaptive meshing was implemented to refine the mesh in the vicinity of weld path by splitting the original existing elements during analysis. A refinement level of 2 is used and heat source area is treated as refinement criterion. The criterion is set by means of a scaling factor which is a multiplier of the heat source size

28

for the local refinement area around the heat source. A scaling factor of 2 has proven to be reasonable for the accurate analysis in this work.

The lower-arm FE model contains 15,405 eight-node hexagonal elements and 31,816 nodes. Due to complexity of the geometry of the welded parts, they are meshed with global element size of 0.5 mm. The upper part contains 8,164 elements and lower part contains 6,323 elements. The three sub-welds contain 414, 216 and 288 elements, respectively. Since the mesh is already very dense, no further mesh refinement was applied in this model.

As mechanical boundary conditions, four clamps were used on the top surfaces of the plates (Figure 3.6) for the lap-joint FE model. The clamps were released during cooling process to allow stress relief and deformation. Four bearing supports were placed exactly at the same positions of the clamps but on the bottom surfaces of the plates. The holding force of clamps was set equal to 500 N.
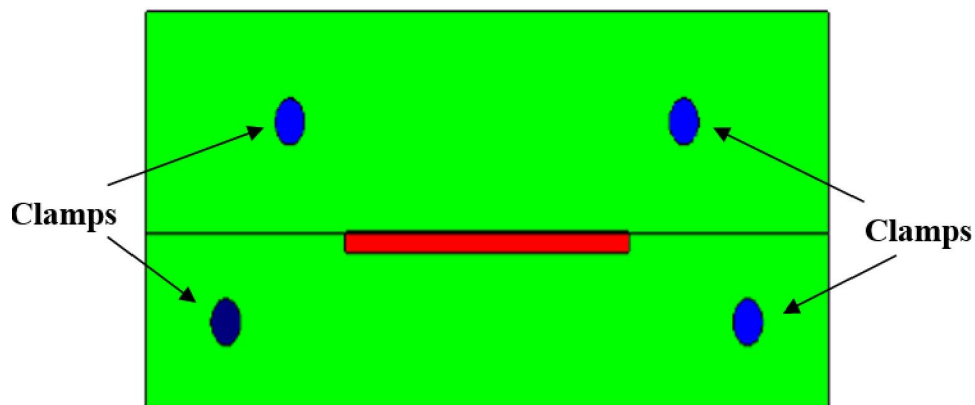
Figure 3.6   Mechanical boundary conditions used in the lap-joint model

For lower-arm FE model, four clamps designed by F.tech engineers were implemented as shown in Figure 3.7.
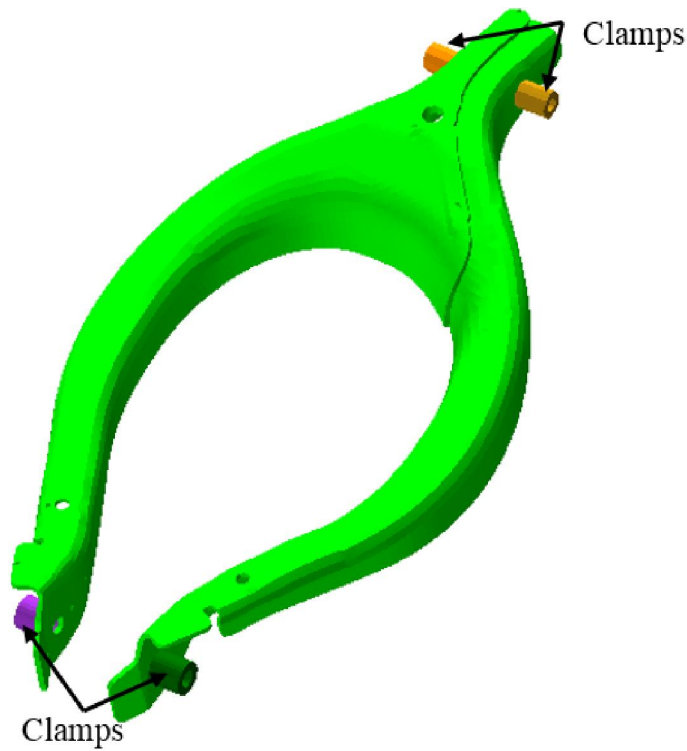
Figure 3.7   Mechanical boundary conditions used in the lower arm model

All the geometries corresponding to mechanical boundary conditions are treated as rigid bodies during simulation and they are made of only thermal elements. As thermal boundary conditions, heat transfer due to convection, radiation and contact with fixtures are considered. The relevant parameters are given in Table 3.1. Same parameters are used for both models.

Table 3.1   Heat transfer coefficients

Coefficient name	Value
Convective heat transfer coefficient, h	20 W/m^2.K
Contact heat transfer coefficient, α	100 W/m^2.K
Emissivity factor, ε	0.6

3.3.3   Heat Source Parameters

The three-dimensional double ellipsoid heat source model [41], is used to simulate the arc welding heat input. As a non-axisymmetric heat source, the front half of the source is one quadrant of an ellipsoid and the rear half is one quadrant of another ellipsoid as shown in Figure 3.8. The Gaussian heat flux distribution is used along the longitudinal axis of the heat source model. The heat source model is defined by four parameters:

- **a$_f$** = the front length of the heat source

- **a$_r$** = the rear length of the heat source

- **b** = the width of the heat source. The total width is 2 b

- **d** = the depth of the heat source.

In this heat source model, the Gaussian power density distribution is shared by the two quadrants and the sharing portions are defined by fraction factors (f$_f$ & f$_r$). Thereby, the power density distribution inside the front quadrant is defined as

$$q_f(x,y,z) = \frac{6\sqrt{3}f_f.Q}{b.d.a_f.\pi.\sqrt{\pi}} e^{\left(\frac{-3x^2}{a_f^2}\right)}.e^{\left(\frac{-3y^2}{b^2}\right)}.e^{\left(\frac{-3z^2}{d^2}\right)}$$

(3.6)

Similarly, for the rear quadrant, the distribution of power density is defined as

$$q_r(x,y,z) = \frac{6\sqrt{3}f_r.Q}{b.d.a_r.\pi.\sqrt{\pi}} e^{\left(\frac{-3x^2}{a_r^2}\right)}.e^{\left(\frac{-3y^2}{b^2}\right)}.e^{\left(\frac{-3z^2}{d^2}\right)}$$

(3.7)

31

In these equations, Q is the heat available at the source, which for an electric arc, it is

defined as

$$Q = \eta V I \qquad (3.8)$$

The heat source dimensions are adjusted to obtain the correct heat flux input and correct

shape of the melted zone. The parameters used in the simulation are shown in Table 3.2.
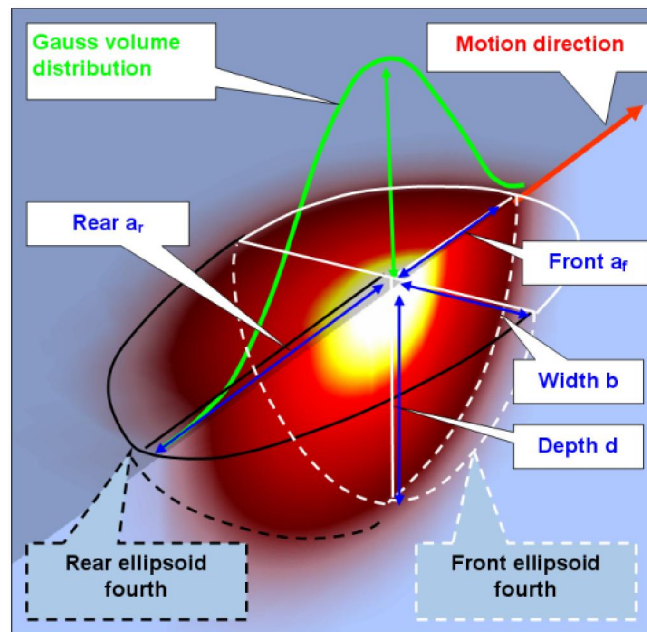
Figure 3.8   Double ellipsoid heat source configuration [64]

Table 3.2   Heat source parameters for both models

	Lap Joint Model	Lower Arm Model
Welding Speed, V (mm/s)	10.0	15.0
Power (W)	4100	2500
Efficiency	80%	90%
Front Length, a_f (mm)	1.00	1.0
Rear Length, a_r (mm)	4.00	1.0
Width, b (mm)	3.25	2.5
Depth, d (mm)	4.00	2.25
Heat Front Scaling Factor, f_f	0.40	1.00
Heat Front Scaling Factor, f_r	1.60	1.00

Heat source parameters, mesh size and time step have critical relationships in transient FEA of the welding process. The total analysis time is divided into many individual time steps (transient analysis). If integration points of an element are not touched by the moving heat source during the specific time step, no heat will be added to the element. This means that time step, speed and element size should suit each other in order to achieve the best possible analysis results. In general, time step can be calculated using the following equation

$$\Delta t = \frac{L}{2^n * V} \tag{3.9}$$

where Δt is the time step, L is the element size along the weld path, n is the refinement level and V is welding speed. The calculated time step for the lap-joint specimen is 0.125 s. For the lower-arm specimen, an adaptive time step automatically adjusted by the solver is used.

3.3.4   Material Modeling

The material of the lap-joint FE model is ASTM A591M-89 sheet metal steel. The material model used in the simulation included relevant temperature dependent thermal and mechanical properties as illustrated in Figure 3.9(a) and Figure 3.9(b), respectively. For the lower-arm FE model, since no experiment was conducted, the same material model was used.
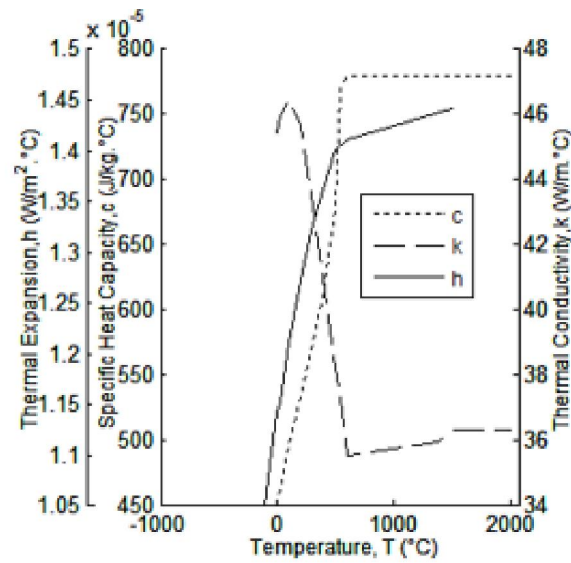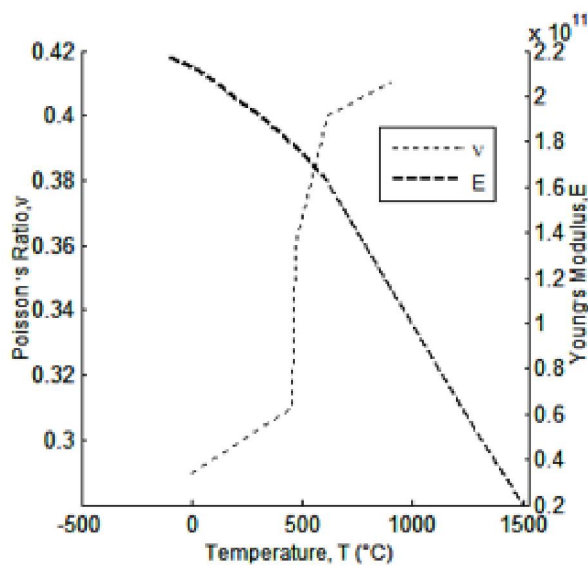
Figure 3.9   Temperature dependent material properties of ASTM A591 sheet metal
             steel-

(a) thermal properties and (b) mechanical properties

3.3.5   FE Welding Simulation

Three-dimensional thermo-mechanical FE simulations were carried out using

Marc solver of simufact.welding©. Since the mid-1970s, Marc has been recognized as

the premier general-purpose program for nonlinear FEA. Marc uses a staggered solution

procedure in coupled thermo-mechanical analysis, where it first performs a heat transfer

analysis, then a stress analysis [65]. The dynamic creation of fillet material is achieved by

the deactivated element method, where elements are first deactivated along the weld path,

then revived as the moving heat source touches any of the integration points of the

elements.

3.4   Welding Simulation Results and Discussion

3.4.1   Lap Joint Model

The simulation time required to run the complete coupled thermo-mechanical

analysis for the lap-joint FE model was approximately two hours using a PC with 2.30

GHz Intel (R) Core(TM) i5-2410M CPU with 8 GB Ram. The welding parameters used

has been shown in Table 3.3. The total simulation time was 137 s in which welding time

was 7 s and cooling time was 130 s. A cooling period of 130 s was sufficient because

distortion did not vary significantly after this time period.

Table 3.3   Welding parameters used for lap joint model

Arc voltage (volt)	20.5
Input current (Ampere)	200.0
Welding speed (mm/s)	7.0

The main driving force in welding simulation is heat generation process. Thus, to

predict the behavior of a weld in a structure, the transient temperature field driven by the

weld heat source must be computed with sufficient accuracy [8]. Lindgren [11] stated that

if the weld pool boundary is correct, then temperature field outside this region will also

be correct. In this work, the heat source model was validated with respect to the weld macrograph (Appendix A) of experimental weld cross sections and a fairly good agreement was achieved in terms of weld pool boundary shape and size as shown in Figure 3.10.
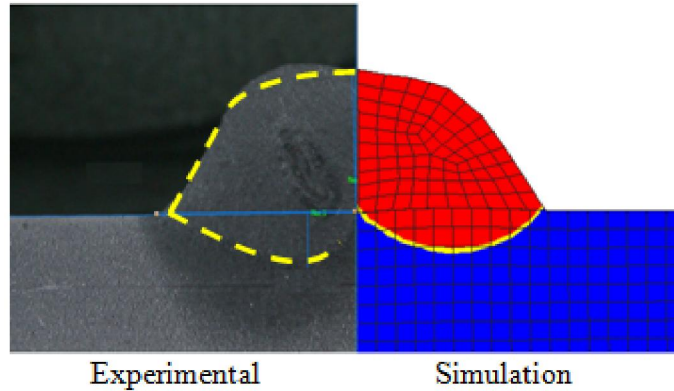
Figure 3.10   Weld pool molten zone shape comparison for the lap-joint model

The typical simulation predicted temperature field across the cross-section of the weld bead can be seen in Figure 3.11. The figure confirms that heat flow in the transverse direction dominates during welding. Also, it is observed that welding quality is sufficiently good since the temperature in the vicinity of the weld pool is above material melting point temperature (around 1400 °C).
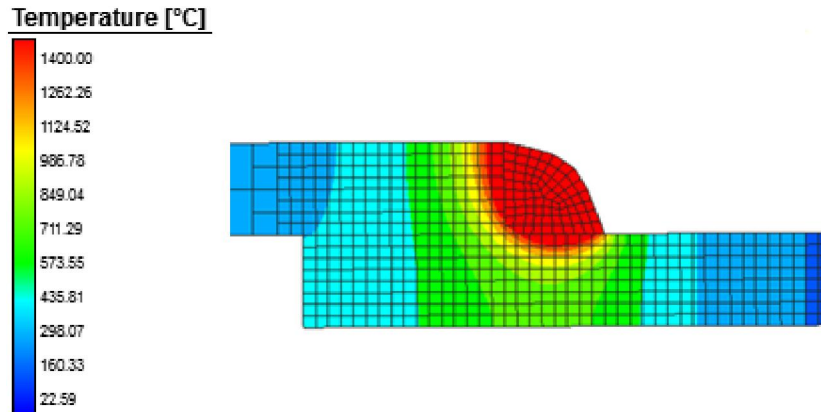
Figure 3.11   Temperature field across the weld bead of the lap-joint model
(35 mm from weld start point)

A basic idea about heat generation and dissipation history can be achieved by the
plot of peak temperature vs time as shown in Figure 3.12. During the experiments, the
temperature was recorded until the peak temperature reached 80 °C. It took around 137 s
for the part to be cooled down to the temperature of 80 °C. As shown in Figure 3.12,
simulation predictions agree fairly well with the experiments during the cooling phase (7
s – 157 s), but around 10-15% discrepancy is observed for the welding phase (0 s – 7 s).
This may be due to some limitation of the experimental temperature measurement device.
The device could not measure temperatures above 1300 °C. Since the material melting
point was around 1400 °C, the peak temperature during welding phase is supposed to be
around 1400 °C or more. However, this discrepancy has little effect on distortion
prediction. Temperatures above the range (600 °C - 800 °C) have minimal effect on
distortion and residual stress for low alloy steel structures [8].

38
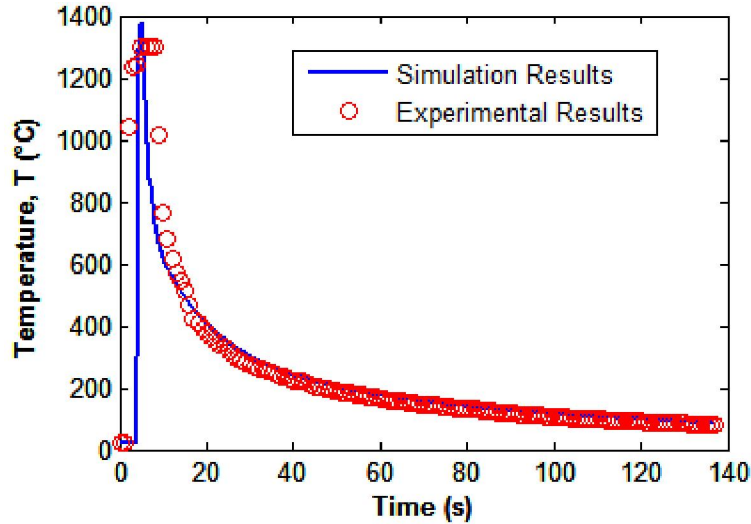
Figure 3.12   Peak temperature history plot of the lap-joint model

After validating the heat source, the simulation predicted out-of-plane distortion was compared with the experimental results by contour plots. Figure 3.13 shows the contour plot of experimental out-of-plane distortion. The maximum positive distortion has occurred in the middle section along the edge of the lower plate (Fig. 3.13) and its magnitude is 0.53 mm. The maximum negative out-of-plane distortion is 0.401 mm. Figure 3.14 shows the out-of-plane distortion pattern predicted by welding simulation. The maximum out-of-plane distortion obtained by simulation was 0.49 mm and 0.35 mm, respectively in positive and negative z axis. The comparison of contour plots indicates that almost similar out-of-plane distortion patterns are achieved by welding simulation and experiments. A more detailed view of distorted shapes of both plates are shown in Figure 3.15. As shown in Figure 3.15, the upper plate is distorted into a convex shape after complete cool down where its high ends are separated from the lower plate. On the other hand, the lower plate is distorted into a concave shape where its middle section

39

towards edge has moved up after complete cool down. The simulation prediction is scaled five times for better visualization purpose.
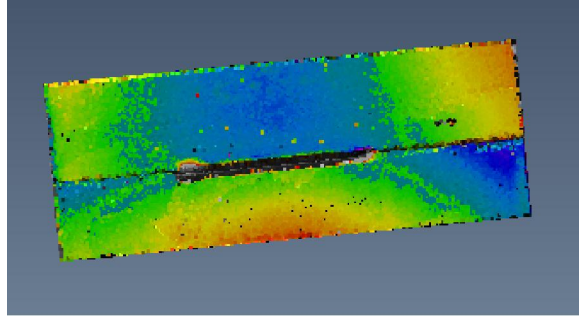
Figure 3.13   Experimental out-of-plane distortion pattern of the lap joint model (in mm unit)
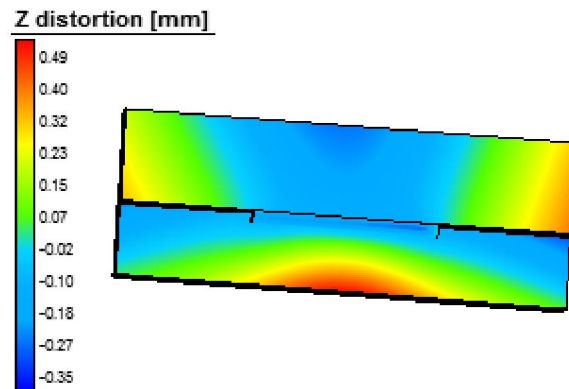
Figure 3.14   Simulation predicted out-of-plane distortion pattern of the lap-joint model (in mm unit)
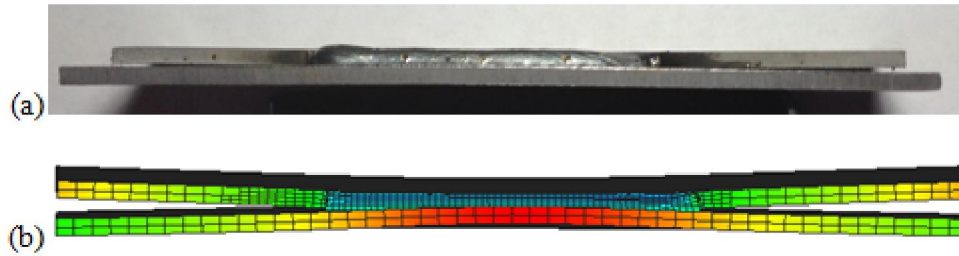
Figure 3.15   Distortion trends of plates

(a) experimental model (b) simulation model

To compare out-of-plane distortion quantitatively with the experiments, three different lines along the two edges and along the midpoint of the weld were considered as shown in Figure 3.16. It is worth mentioning that the laser scanner used in the experiments recorded thousands of data points over the surface with a reference frame not identical with the simulation model. As such, it was not possible to compare distortions at exactly the same positions for both the experimental and simulation models. The experimental data points have been picked up randomly and thereby some deviation from the exact line has occurred during manual point selection. Although there is some discrepancy between the experimental and simulation results, the general trend of the plots indicates that the simulation predictions are sufficiently accurate on the basis of quantitive comparison as well.
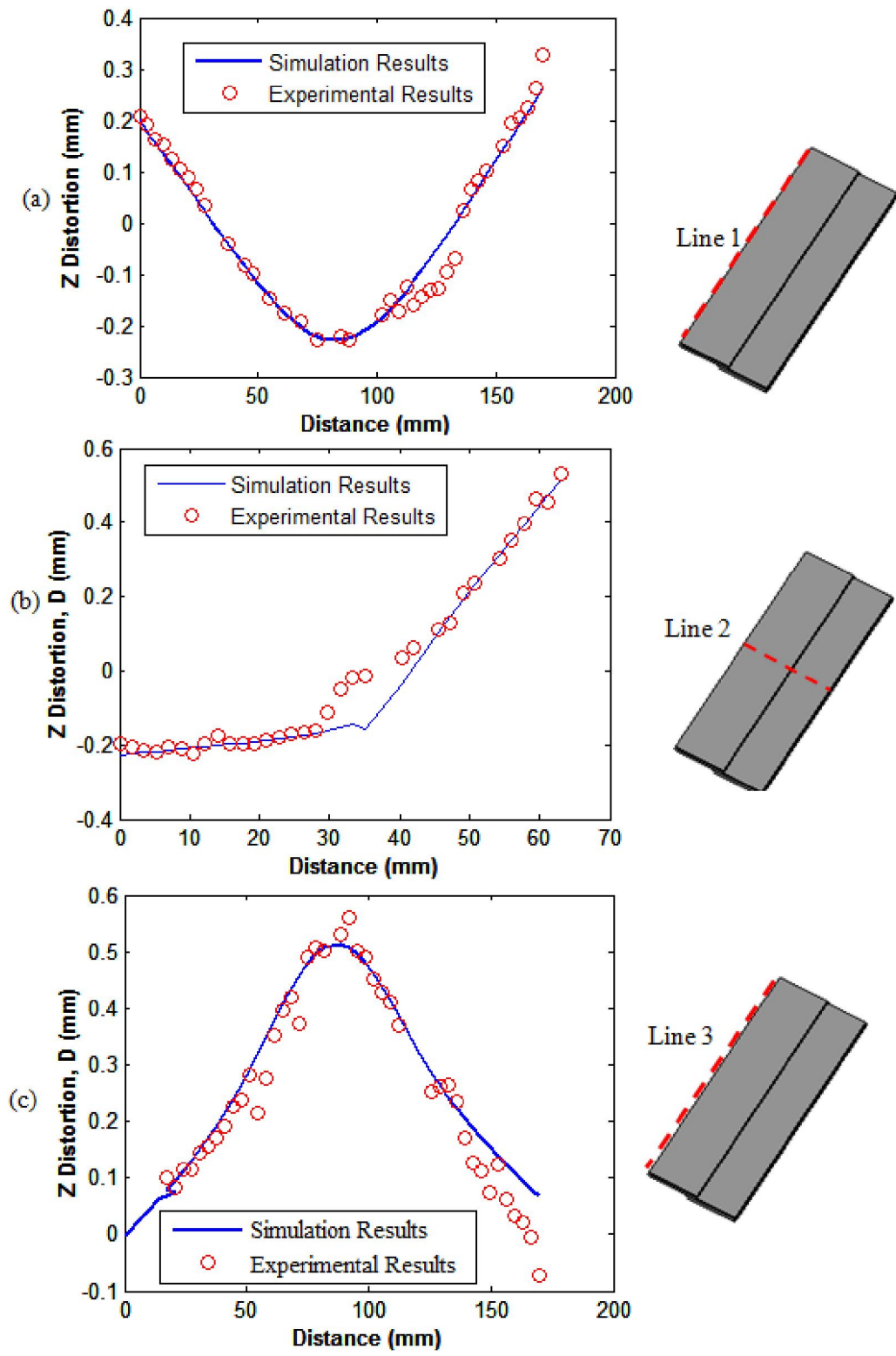
Figure 3.16   Quantative Comparison of out-of-plane distortion along different sections-

(a) line 1 , (b) line 2 and (c) line 3

Furthermore, total distortion pattern obtained by simulation is shown in Figure 3.17. The maximum distortion (0.58 mm) has occurred in the middle section of the lower plate. Also, due to contact separation, the left end of the upper plate shows larger distortion value that is greater than 0.5 mm.
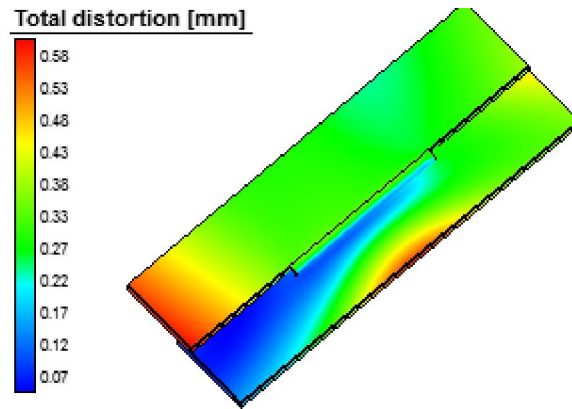
Figure 3.17   Simulation predicted total distortion pattern (in mm unit)

Next, the residual stress distribution over the plates was investigated. Figure 3.18 shows the longitudinal residual stress distribution along the middle section of welding on the top surface of the model after cooling down of the structure to 80°C. Figure 3.18 (a) shows the distribution of longitudinal residual stress (σ_y) on the top surface of the model. Tensile residual stress of high magnitude is produced in the region near the weld and it decreases rapidly over a distance far from the weld line and becomes compressive towards the edges of the plates. Since the model is not symmetric with respect to the weld line, the stress distribution is also unsymmetric as well. It is observed that the maximum tensile and compressive longitudinal residual stresses are 460 MPa and 136 MPa, respectively. The distribution of transverse residual stress (σ_x) along the length of weld

43

on the top surface of both plates is illustrated in Figure 3.18 (b). For the upper plate, tensile stress of relatively low magnitude is produced in the middle section of the joint and compressive stress is produced at both ends of the joint. The maximum tensile and compressive transverse residual stresses for upper plate are 42 MPa and 130 MPa, respectively. However, for the lower plate, relatively high transverse residual stress but less than longitudinal tensile residual stress is produced in the middle section of the joint and also higher compressive stress is produced at both ends of the joint. The maximum tensile and compressive transverse residual stresses for lower plate are 235.2 MPa and 212.7 MPa, respectively.
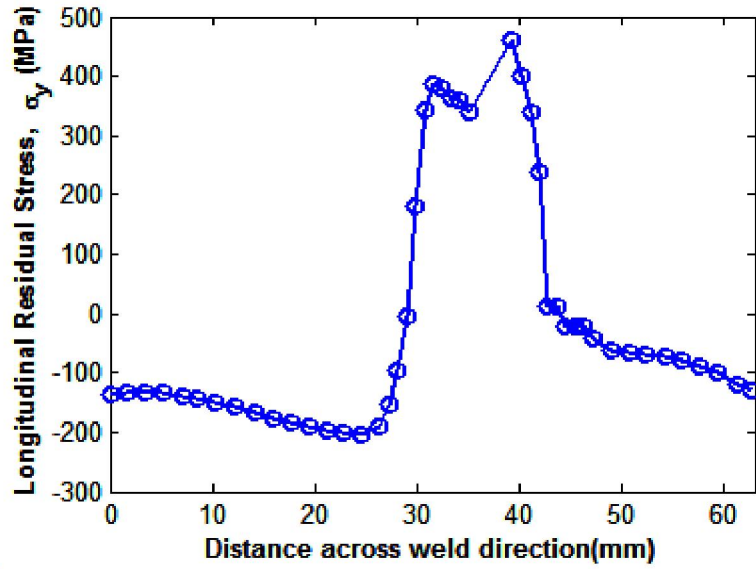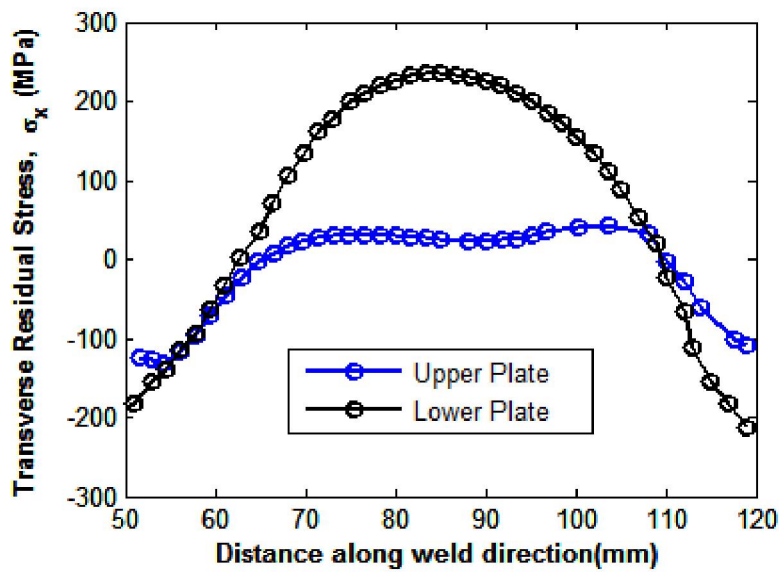
Figure 3.18   Residual stress plots of the lap-joint model-

(a) longitudinal residual stress plot and (b) transverse residual stress plot

Since the weld bead is directly deposited over the top surface of the lower plate, a

greater portion of the intense and non-uniform thermal load caused by welding is

transmitted to the lower plate. As such, the phenomenon of relatively higher transverse

residual stress in the lower plate can be attributed as a consequence of the higher thermal load on the lower plate. Moreover, a contour plot of the effective stress over the entire structure also supports the fact that the lower plate is subjected to higher residual stress than the upper plate as shown in Figure 3.19.
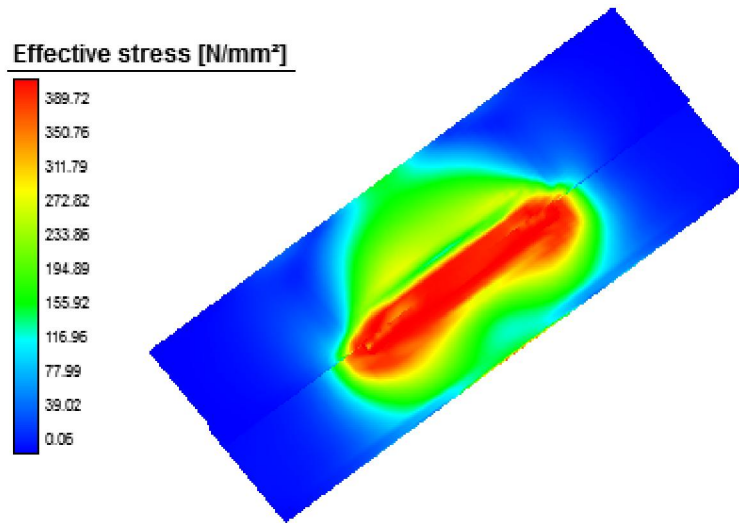
Figure 3.19   Contour plot of effective stress over the top surface of the lap-joint model

3.4.2   Lower Arm Model

The simulation time required to run the complete decoupled thermo-mechanical analysis for the lower-arm FE model was approximately four hours on a PC with a 2.30 GHz Intel (R) Core(TM) i5-2410M CPU with 8 GB Ram. It is to be noted that this model could not be validated due to unavailability of any relevant prior experimental or simulation works on this particular model. However, based on previous validation experience, a good effort was made to make the simulation model as accurate as possible. The welding parameters used for this model are given in Table 3.4.

Table 3.4   Welding parameters used for lower arm model

Arc voltage (volt)	18.0
Input current (Ampere)	180.0
Welding speed (mm/s)	15.0

The total simulation time was 50 s in which welding time was 10 s approximately and cooling time was 40 s. As the first step of modeling, the heat source model was calibrated to obtain sufficiently accurate weld pool shape. The fillet element was modeled as triangular shaped weld bead with the resultant molten weld pool shape for subweld 1 depicted in Figure 3.20. The red zone indicates that temperature of the portion is above the melting point.
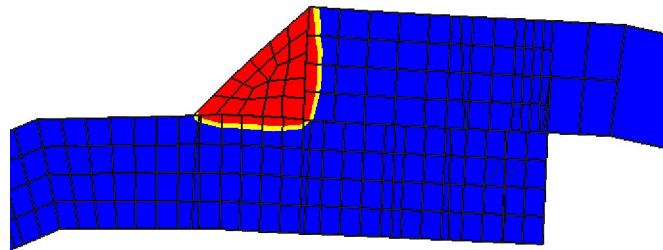
Figure 3.20   Typical weld pool shape of the lower-arm FE model

The typical simulation predicted temperature field across the cross-section of the weld bead can be seen in Figure 3.21. It is observed that welding quality is sufficiently good since the temperature in the vicinity of the weld pool is above or close to material melting point temperature (around 1400 °C). An idea of typical fusion zone and heat affected zone can be achieved from this contour plot.
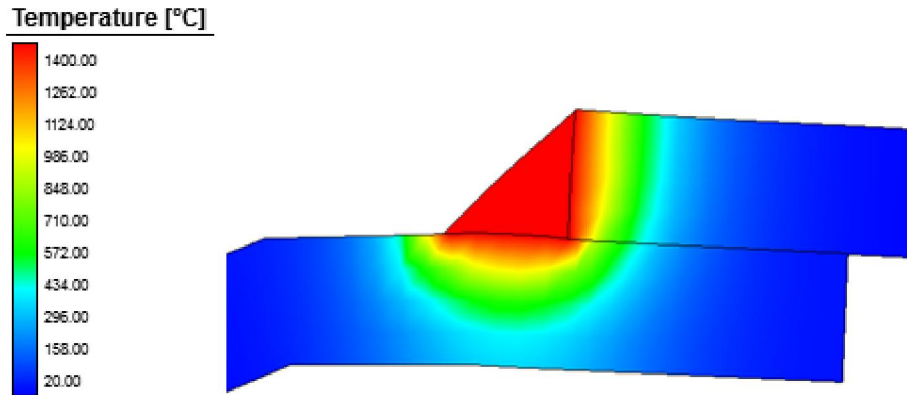
Figure 3.21   Temperature field across the weld bead
(7.5 mm from weld start point)

Figure 3.22 shows the temperature variation of three representative times during
welding (5 s), just after welding (15 s) and at the end of analysis (50 s). As shown in the
figure, peak temperature generated during welding process is around 1450 ⁰C and after
the end of analysis (50 s), peak temperature is around 170 ⁰C.

| (a) | (b) | (c) |
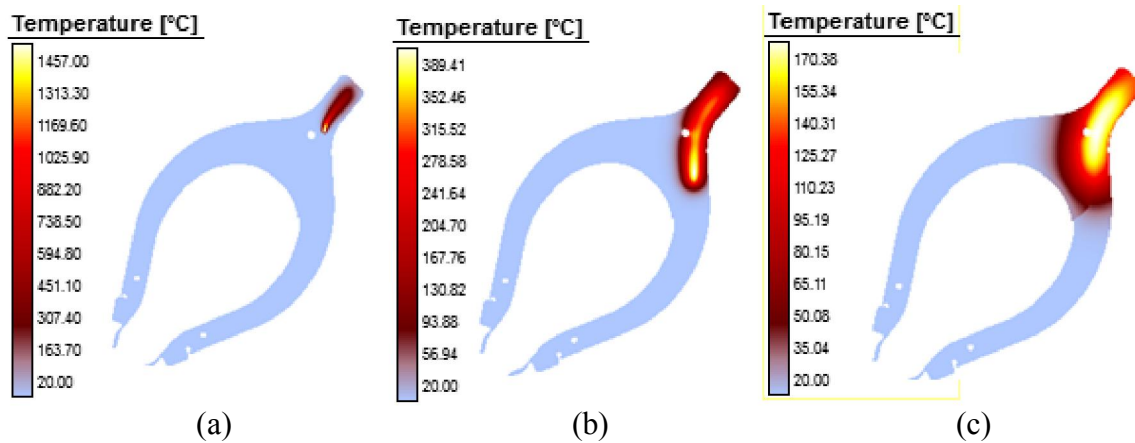
Figure 3.22   Surface temperature distribution in the lower arm at different time
                intervals-

(a) time = 5s, (b) time = 15s and (c) time = 50s

After calibrating the heat source model and performing thermal analysis, the residual stress distribution over the top surface of the lower arm was investigated. Figure 3.23 shows the evolution of longitudinal normal stress denoted by Y normal stress along the cross-sections of the sub-welds normal to the welding direction. As shown in the figures, tensile stress of high magnitude is produced in the region near the weld and it decreases rapidly over a distance far from the weld line and becomes compressive in nature. It is observed that intensity of longitudinal normal stress gradually reduces as the welding arc moves along the weld path. The maximum tensile and compressive longitudinal normal stresses are 578 MPa and 529.76 MPa, respectively.
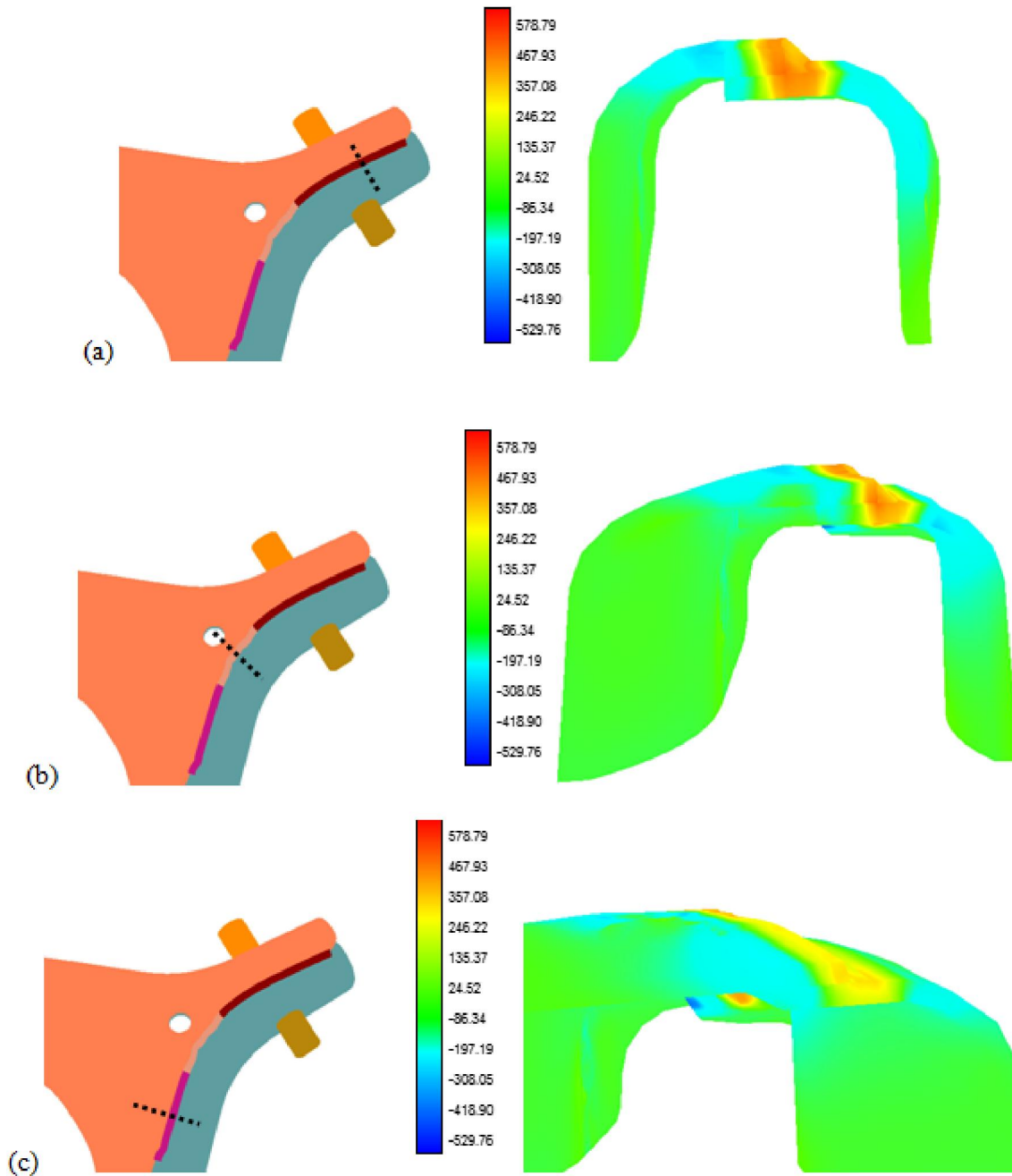
Figure 3.23   Contours of longitudinal normal stress (MPa) along different cross sections-

(a) sub-weld 1, (b) sub-weld 2, (c) sub-weld 3.

Next, the simulation predicted distortion was investigated by contour plots. Figure 3.24 shows the typical comparison of distorted shape of the structure with the initial

50

undistorted structure. The distorted shape is magnified 10 times for better visualization. The distortion pattern of the structure indicates that the lower part has undergone higher distortion than the upper part due to direct deposition of weld metal on it. The maximum distortion has occurred at the middle section of the lower part and its magnitude is 0.59 mm.
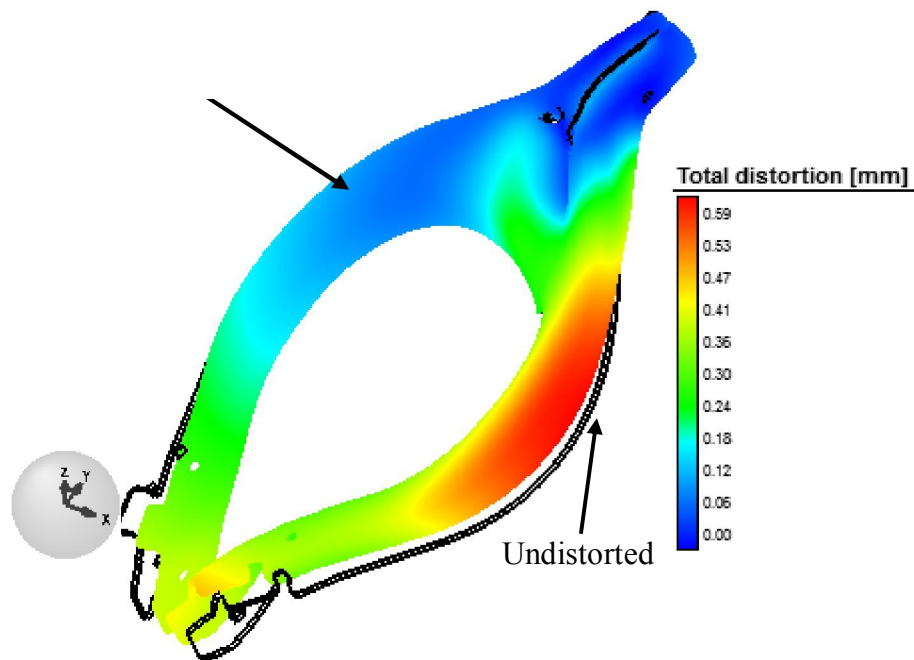
Figure 3.24   Comparison of distorted and undistorted shapes of the lower-arm model

Furthermore, distortion components along each of the three directions are shown in Figure 3.25. An analysis of distortion component along the z axis indicates that the lower part has a tendency to move up in the middle section in response to the thermal load applied by welding. Also, the bottom sections of the both parts have movement tendency in the x direction.
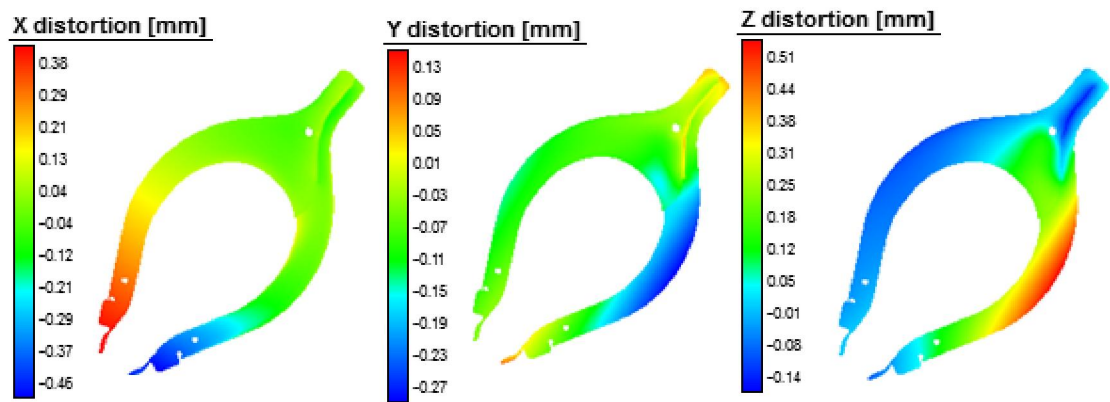
Figure 3.25   Distortion components along the three axes of the lower-arm mode

CHAPTER IV

COMPUTATIONAL OPTIMIZATION METHODOLOGY

4.1   Background of Design Optimization

Design optimization can be defined as a systematic process by which a measure of objective function (e.g., weight, cost, strength, deflection) is optimized (minimized or maximized) by varying the design variables while satisfying all the design constraints (i.e., requirements and limitations) [65]. Although all optimization methods deal with mathematical models, it is also possible to achieve optimum design through physical or numerical experiments. The general approach to describe a design optimization problem is as follows

$$\min f(\mathbf{X})$$
$$\text{subject to} \quad g_j(\mathbf{X}) \leq 0 \quad j = 1 \text{ to } N_g$$
$$h_k(\mathbf{X}) = 0 \quad k = 1 \text{ to } N_k \tag{4.1}$$
$$X_i^l \leq X_i \leq X_i^u \quad i = 1 \text{ to } N_{DV}$$

where $f(\mathbf{X})$ is the objective function, $\mathbf{X}$ is the design variable vector, N_g and N_k are the number of inequality $g_j(\mathbf{X})$ and equality $h_k(\mathbf{X})$ constraints, respectively. The lower and upper bounds of a design variable are defined by X_i^l and X_i^u, respectively.

In simulation-based design optimization, the objective function and constraints are evaluated by numerical methods such as FEA. In such cases, the mapping from

53

design variables to objective function and constraints is strictly implicit. The implicit relationship is essentially evaluated by a "black box" computational model and thereby it is hard to judge whether these functions are continuous and differentiable as the convergence conditions of some optimization methods (i.e., gradient-based methods) require. Gradient-based methods, thus, may not be appropriate for these optimization problems. Derivative-free techniques such as Genetic Algorithms (GA) can be easily adopted in these problems. GA requires only objective function values and thereby it has the ability to handle problems in which the objective function is discontinuous, nondifferentiable, stochastic, or highly nonlinear. In fact, it is independent of the objective function definition for which it can be easily integrated with "black box" computational models for objective function evaluation. It can also treat discrete and/or continuous design variables allowing greater design flexibility during optimization. As such, it is very suitable for a nonlinear and unorthodox optimization problem like welding process parameter optimization via FE simulation.

Despite the steady growth in computing power, the complexity and high cost of FEA seem to keep pace with computing advancement [66]. As such, it may not be feasible to conduct iterative optimization directly using computation intensive simulations for objective function evaluations as this may greatly increase the overall design cost. The common approach to deal with this problem is to carry out a number of computer simulations based on Design of Experiments (DOE) method and develop an inexpensive model approximating the relationship between input variables and desired responses. Models that are cheaper representations of a more complex ones are referred to as surrogate models or metamodels [66]. If we assume the true response of a

54

simulation model is y = f(x), the response of its corresponding metamodel is represented

by $\hat{y} = \hat{f}(x)$ so that $y = \hat{y} + \varepsilon$, where ε is the error of approximation. Subsequently,

the formulation of the optimization problem is modified to

$$\min \hat{f}(\mathbf{X})$$

$$\text{subject to} \quad \hat{g}_j(\mathbf{X}) \leq 0 \quad j = 1 \text{ to } N_g$$

$$\hat{h}_k(\mathbf{X}) = 0 \quad k = 1 \text{ to } N_k \qquad (4.2)$$

$$X_i^l \leq X_i \leq X_i^u \quad i = 1 \text{ to } N_{DV}$$

Metamodeling process involves four steps [66]: (1) selecting a DOE method or

the way to systematically conduct the experiments and generate the response data, (2)

choosing a model to represent the data, (3) fitting the model, and (4) validating the model

from the observed data obtained in the first step. Although there exists several methods

for each of these steps, the most frequently used methods include response surface

methodology (RSM), inductive learning, neural network and kriging method [66]. In this

research work, we have focused on RSM due to its wide acceptance for metamodeling

and simplicity in theory.

4.2   Outline of Genetic Algorithms

A generic GA can be considered as a controlled random walk; it efficiently

exploits information from previous configurations to generate new configurations with

improved performances expected [67]. GA relies on stochastic search techniques based

on the mechanism of natural selection and natural genetics. GA differing from

conventional search techniques, starts with an initial set of random solutions called

population. Each individual in the population is called chromosome, representing a

solution to the problem. The chromosomes evolve through successive iterations, called generations. During each generation, the chromosomes are evaluated using some measure of fitness or cost. To create the next generation, new chromosomes, called offsprings, are formed by either merging two chromosomes from current generation using a crossover operator or modifying a chromosome using a mutation operator. A new generation is formed by selecting, according to fitness/cost values, some of the parents and offsprings and rejecting others so as to keep the population size constant. Chromosomes with better fitness values have higher probability of getting selected. After several generations, the algorithm converges to the population containing the best chromosome, which is assumed to represent the optimum solution of the problem. Typical iterative process of GA is shown in Figure 4.1.
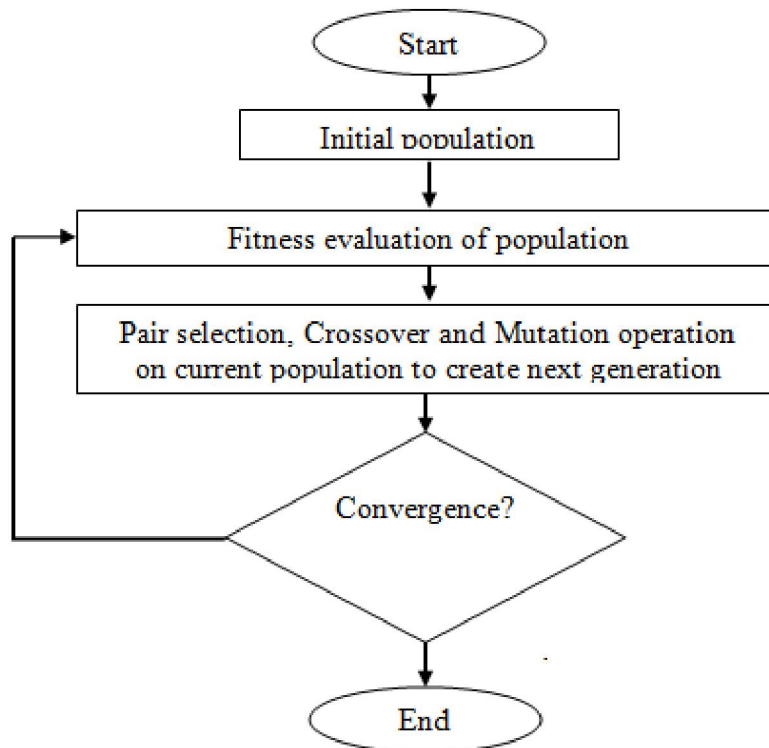
Figure 4.1   Flow diagram of simple genetic algorithm

4.3   Response Surface Methodology

RSM is a collection of statistical and mathematical techniques useful for developing, improving and optimizing processes [68]. It approximates the unknown functional relationship between a response of interest and input variables by a polynomial response surface (PRS). The quadratic polynomial model is the most popular PRS because of its flexibility to take on a wide variety of functional forms, ease of estimating the parameters and several practical success experiences in solving real engineering problems. The mathematical model of quadratic response surface is described as

$$y = \beta_o + \sum_{i=1}^{k} \beta_i x_i + \sum_{i=1}^{k} \beta_{ii} x_i^2 + \sum_{i=1}^{k-1} \sum_{j=k+1}^{k} \beta_{ij} x_i x_j + \epsilon \qquad (4.3)$$

where k is the number of variables, ε is the error and βs are the constant regression coefficients. The quadratic model in Eq. (4.1) includes $p = (k+1)(k+2)/2$ unknown coefficients (β_0, β_i, β_{ii}, and β_{ij}) that are found using the least squares technique based on the true response values at a set of $n \geq p$ training points.

Various DOE techniques such as Latin Hypercube (LHS), Taguchi orthogonal arrays, Central Composite Design (CCD) and Box-Behenden Design may be used for identifying the training set in the design space bounded by the lower and upper bounds of x_i, $i = 1$, k. The accuracy of a surrogate model is dependent on the number of training points and how these training points are distributed in the design space. For a PRS, at least *3k* training points are necessary to build a good surrogate model [68].

4.4 Optimization Problem Formulation

4.4.1 Lap-Joint Model Optimization

In this work, the goal is to reduce the weld induced distortion. Thus, the maximum distortion is treated as the objective function. Through welding simulation, distortions in all nodes (N) are first calculated as the sum of square roots of nodal distortions in all three directions. Then, the maximum distortion value is selected and used as the objective function value for iterative optimization via GA. Thus, the objective function is defined as

$$F(X) = \max(D_i)$$

$$\text{where } D_i = \sqrt{(d)_i^2 + (d_y)_i^2 + (d_z)_i^2} \quad i = 1,2,3 \dots N$$

(4.4)

The design variables and corresponding bounds are defined in Table 4.1.

Table 4.1   Description of process design variables of the lap-joint model

Lap Joint Model					
Design Variable	Definition	Unit	Lower Bound	Upper Bound	Increment
X1	Current	Ampere	80	250	80,100,120,..., 250
X2	Voltage	Volt	8	25	8,10,12,..., 25
X3	Welding Speed	mm/s	3.5	10	3.5,5,7,10
X4	Welding Direction	-	1	6	1,2,…, 6

For the lap-joint model, X4 can take six numerical values to represent six possible welding directions as shown in Figure 4.2. Two welding directions are designed with one robot and they are represented by integer values 1 and 2, depending on robot's left-right or right-left movement direction, respectively. Similarly, the remaining four welding directions are designed with two robots and they are represented by an integer from 3 to 6 depending on each robot's left-right or right-left movement direction. For the two robot welding cases, it was assumed that both robots will start and stop welding at the same time.
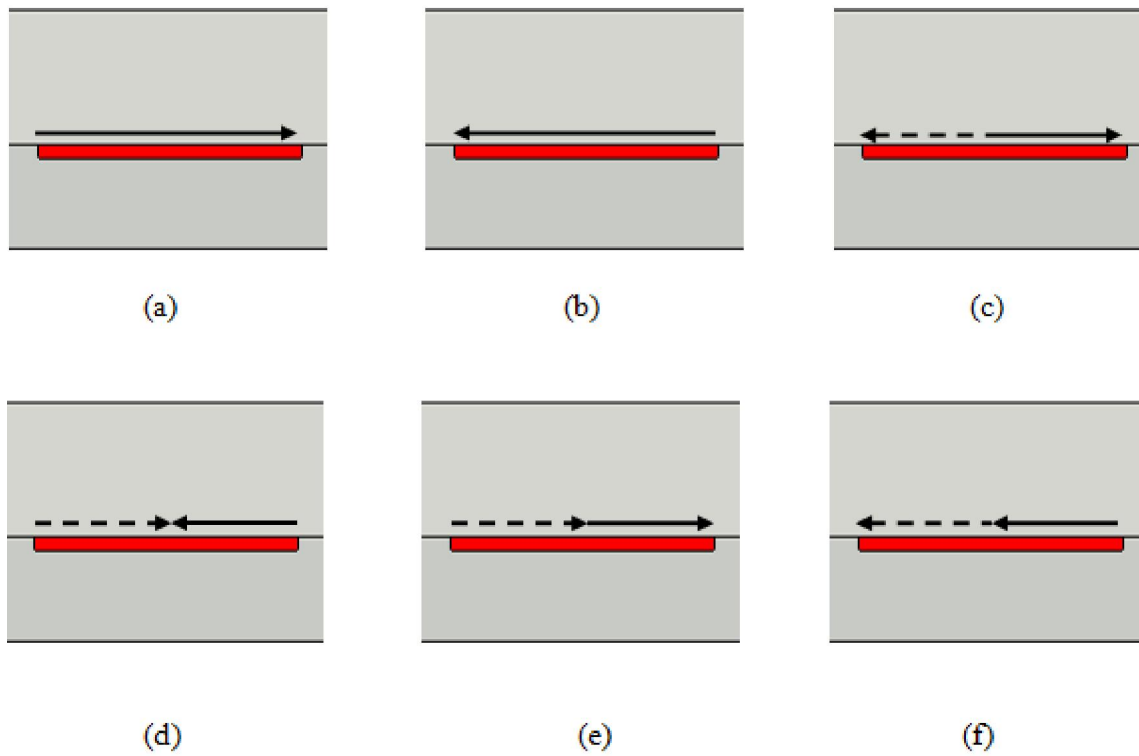
Figure 4.2   Definition of welding direction variable, X4 values-
(a) X4=1, (b) X4 = 2, (c) X4= 3, (d) X4= 4, (e) X4 = 5 and (f) X4 = 6

During optimization process, GA picks design variable values automatically. As such, it is very likely that it will often pick values that will result in poor welding quality. For example, if the heat input (current x voltage) is very low, welding quality will be poor due to incomplete fusion or insufficient weld penetration as shown in Figure 4.3.

(a)   (b)
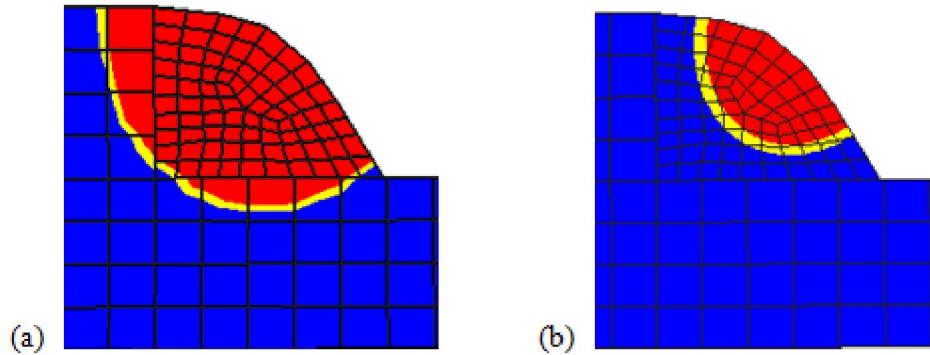
Figure 4.3   Effect of heat input parameters on welding quality-
(a) good welding and (b) bad welding

To ensure a strong welded joint and good welding quality, it is important that the temperature in the welding zone is higher than or equal to melting temperatures of base metals and weld beads during welding. As such temperature constraints have been used to ensure good weld quality. During FE simulations, temperatures at three different weld bead cross-sections are monitored to check temperature constraints. The tracking sections are illustrated in Figure 4.4.
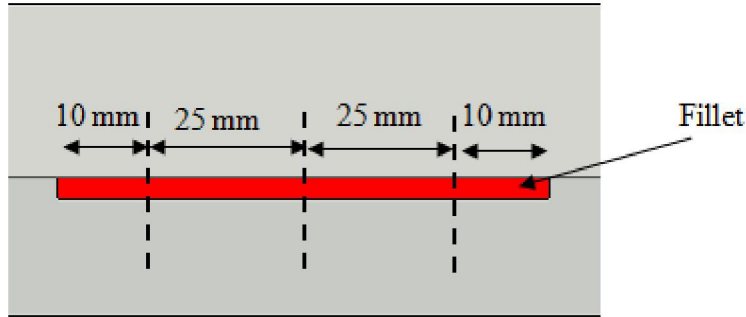
Figure 4.4   Tracking sections (dotted lines) for monitoring temperature constraints

To incorporate the constraint violation into optimization algorithm, a penalty term is added to the objective function and the combined function is called augmented function. Whenever a constraint is violated, the penalty term is greater than zero, with the magnitude of the penalty being proportional to severity of constraint violations. In this work, the penalty term is proportional to the number of fillet element nodes (N_c) that violate the temperature constraint. The augmented objective function definition including optimization constraints is defined as

$$\varphi(x) = \begin{cases} F(X), & N_c = 0 \\ F(X) + 100 * N_c, & N_c > 0 \end{cases} \tag{4.5}$$

The penalty term increases the original objective function value and indicates to GA that the associated model is infeasible. An infeasible model represents poor welding quality even though the weld-induced distortion may be small.

4.4.2   Lower-Arm Model Optimization

For the lower-arm model, the objective function definition is also the same as that in Eq. 4.2. Since the welding path is nonlinear and sufficiently long, the impact of

welding order or sequencing is very critical on weld induced distortion. As such, for this

case study, welding sequences are treated as design variables in conjunction with other

process dependent variables. Dividing the weld path into several sub-welds that are

welded sequentially in a specific order is one of the most important and cost effective

distortion and residual stress mitigation strategies. The order (sequence) by which sub-

welds are welded alters the cooling patterns and as a result alters distortion and evolution

of the residual stresses. The entire weld path is divided into three sub-welds and the order

of occurrence of each sub-weld is treated as design a variable. Therefore, there are six

design variables in this case study, the first three are defined in Table 4.2 and the latter

three representing the sub-weld orders (X4, X5, X6) are shown in Figure 4.5.

Table 4.2   Description of process design variables of lower arm model

Design Variable	Definition	Unit	Lower Bound	Upper Bound	Increment
		Lower Arm Model			
X1	Current	Ampere	100	150	100,110,120,..150
X2	Voltage	Volt	20	25	20,20.5,21,....25
X3	Welding Speed	mm/s	15	22	15,18,20,22
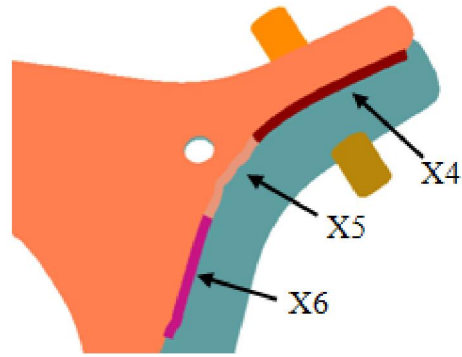
Figure 4.5   Details of sub-weld design variables

The design variables associated with sub-weld orders are treated as discrete design variables. Each sub-weld can occur in three different orders and each can have two directions (forward or backward). Thus, each sub-weld design variable has six discrete status values that it can possess as listed in Table 4.3. For example, if sub-weld 1 occurs at first position and welding is done in forward direction for this sub-weld, then the status of X4 is 1 as shown in Figure 4.6. Total number of combinations (N) possible from three sub-welds is 48 (2^3x3!).

Table 4.3   Details of sub-weld design variables

Design Variable Status	Welding Order	Welding Direction
1	First	Forward
2	Second	Forward
3	Third	Forward
4	First	Backward
5	Second	Backward
6	Third	Backward
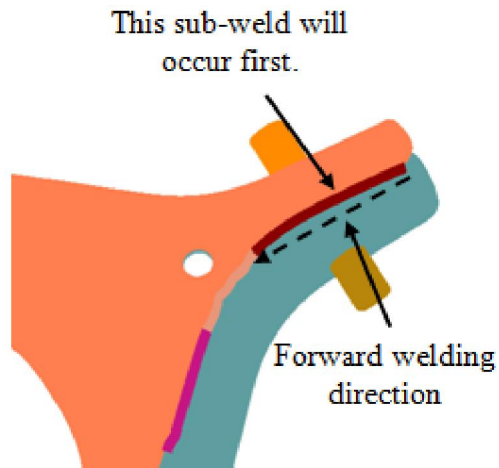
Figure 4.6   Meaning of design variable (X4=1)

Similar to the lap-joint model, temperatures at three different weld bead cross-sections are monitored to check the temperature constraints. The tracking sections are illustrated in Figure 4.7. Also, the corresponding objective function is also converted to the augmented function of Eq. 4.3.
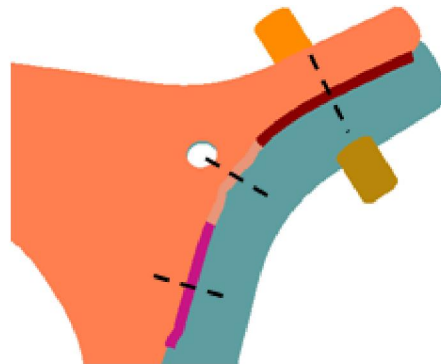
Figure 4.7   Tracking sections (dotted lines) for monitoring temperature constraints

4.5   Genetic Algorithm Based Optimization Procedure

4.5.1   Direct Computational Optimization

The direct optimization initiates GA by creating a random initial population with each individual member of the initial population evaluated by the FEM tool. For example, an individual represents a set of values for welding speed (X1), arc voltage (X2), input current (X3) and welding direction (X4) for the lap-joint model. The program stores each individual and its fitness value so as to ensure not to reevaluate twice the same individual in successive generations. Then, based on the objective function values obtained from simulation output program, GA creates next generation and evaluates this population similarly using FEM tool to search for optimum point. The system algorithm runs until the maximum number of generations is reached or the cumulative change in the objective function value over five generations is less than or equal to predefined objective function tolerance. The advantage of direct simulation-based optimization is that the verification at optimum point is unnecessary. The direct computational optimization approach using GA is shown in Figure 4.8.

4.5.2   Response Surface Model Based Optimization

In this approach, a DOE table is constructed first using the popular Box-Behnken method, and subsequently the response at each design point of the DOE table is evaluated by the welding simulation. After calculating the response values at all the DOE points, a quadratic PRS is developed using the least squares technique. Accuracy of the response surface model largely depends on the number and range of design points in the DOE table. The PRS model is not guaranteed to be adequately accurate in the first trial. As such, an iterative process of DOE table construction-PRS fitting-error checking is carried

out to fit the PRS with adequate accuracy within the design space defined by the DOE

table. Next, the PRS is linked with GA for design optimization. The RSM based

optimization approach using GA is shown in Figure 4.9.
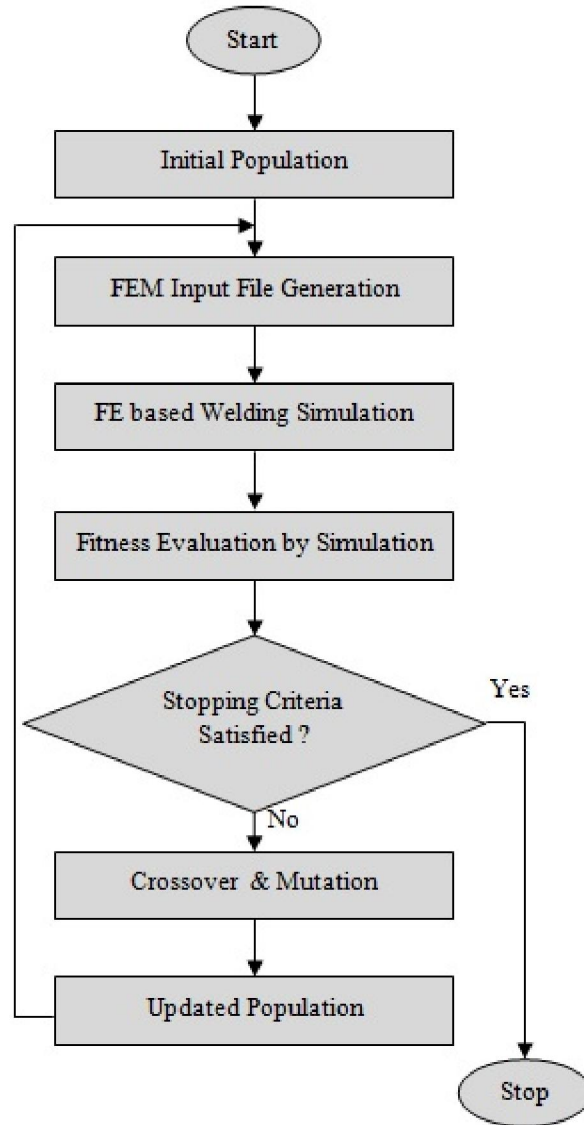
Figure 4.8   Flowchart of direct computational optimization system
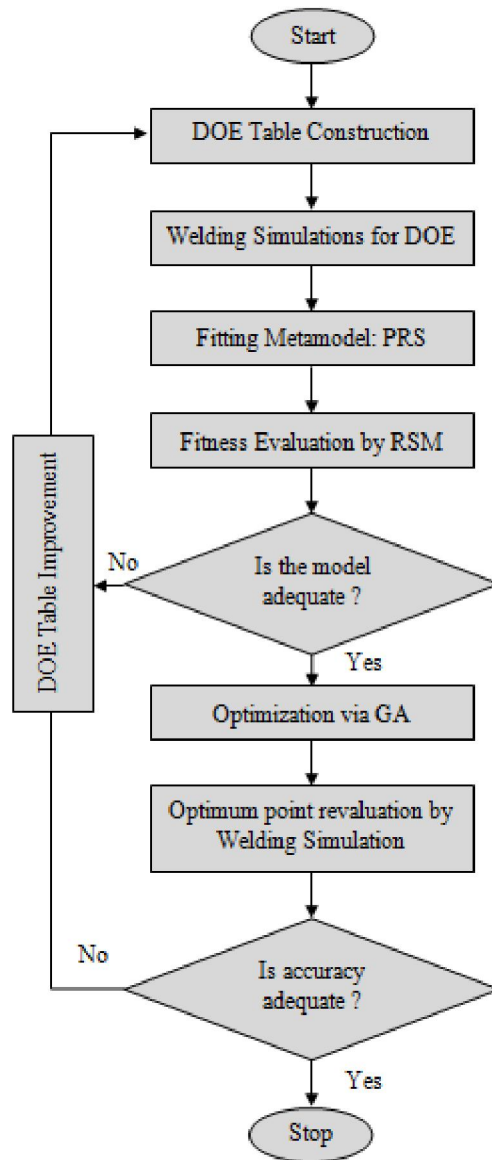
Figure 4.9   Flowchart of RSM based optimization system

4.6   Computational Framework and Software Implementation

The optimization software used in this thesis work is MATLAB® global

optimization toolbox [69]. The GA solver of the toolbox was integrated into the

automatic computational optimization system. MATLAB® GA solver supports algorithm

67

customization. A customized GA variant can be created by varying different default solver properties to meet their problem-specific requirements. The flexibility to customize the GA options was utilized to the greatest extent in integrating the FE based welding simulation tool with GA for simulation-based design optimization. In this work, the functional relationship between design variables and objective function to be optimized is explicit. Therefore, conversion of the original simulation model and its responses into standard mathematic function values recognizable by the fundamental optimization algorithm is the greatest challenge of this investigation. For this purpose, multiple computer programs were developed in the MATLAB® programming environment and linked together to form the computational framework.

The proposed computational optimization framework consists of four computer programs: (1) a welding simulation program, (2) an optimization program, (3) a simulation input generation program and (4) a simulation output evaluation program. The optimization program is the main controlling program of the system. It runs GA to produce a new population of design variable values based on the simulation results of previously evaluated models. It also takes the important decision of stopping the analysis by checking the stopping criteria in each iteration. Furthermore, it also keeps records of results, model information and constraint violations in each iteration. The simulation input program takes new values of design variables as input, inserts those values into the FEA input file and passes the updated input file to the welding simulation program as output. The welding simulation program (e.g., Simufact.welding) executes the welding simulations based on the input file and stores the desired output results. The last program is the simulation output evaluation program which reads the output result files of welding

simulations, extracts the specified results and provides the extracted results to the optimization program as input. The optimization program uses the extracted results to produce new population and in this way the analysis loop repeats until the best solution does not change over a pre-specified number of iterations. The complete computational framework is illustrated in Figure 4.10.
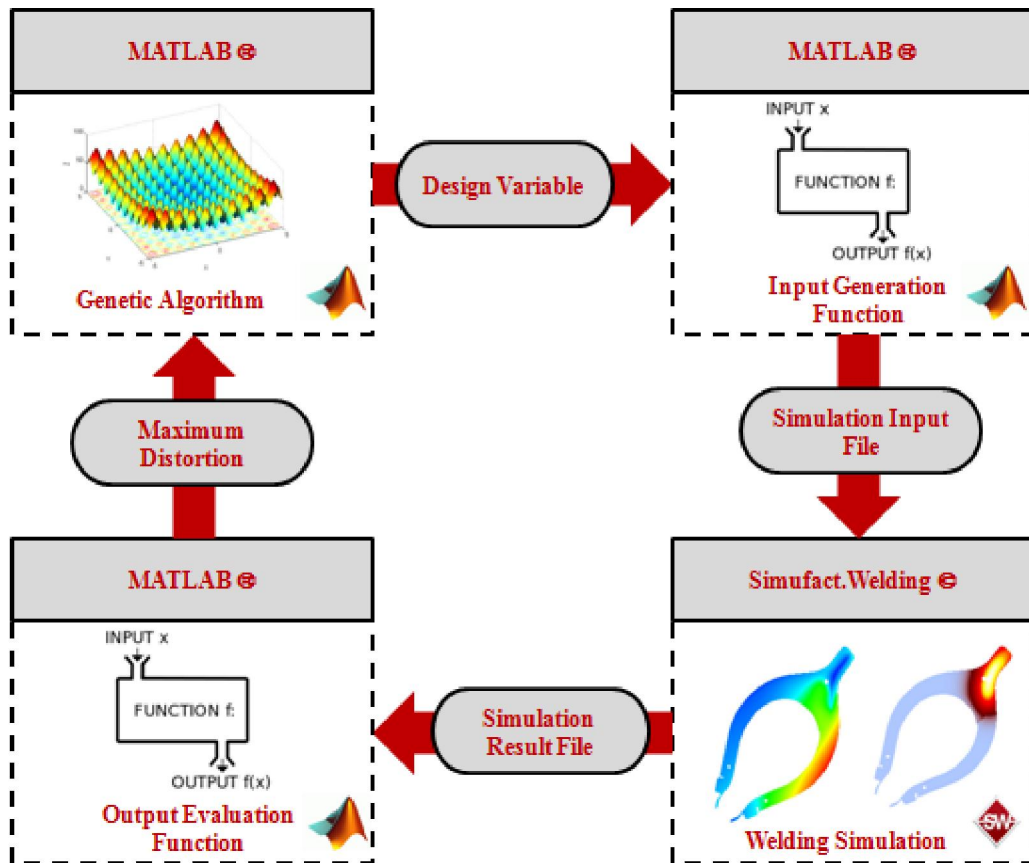
Figure 4.10   Computational design optimization framework for welding process

4.7   Optimization Results and Discussion

4.7.1   Sensitivity Analysis of Lap-joint Model

A two-level DOE-based sensitivity analysis was conducted as a first step to investigate the sensitivity of the chosen output (max weld induced distortion) to the selected design variables (current, voltage, speed and direction). The arbitrarily selected baseline point and its corresponding response are given in Table 4.4. Since welding direction is not a continuous variable, it is difficult to interpret the response of the output to the change in welding direction. Therefore, a separate sensitivity analysis was carried out with the other three design variables for arbitrarily selected welding direction (i.e., $X4$ value). Physical meaning of each welding direction is described in Figure 4.2. The difference of the highest relative to the lowest max distortion value in Table 4.4 is approximately 25%.

Table 4.4   Baseline design variable values and response of the lap-joint model

$X1$, Ampere	$X2$, Volt	$X3$, mm/s	$X4$	Max Distortion, mm
150	15	7	1	0.523
150	15	7	2	0.512
150	15	7	4	0.584
150	15	7	6	0.641

The sensitivity analysis was formulated such that each variable can take either a high or a low value for each design point while the other two variables are kept at their respective baseline values. As such, the calculated sensitivity represents the percentile main effect of each design variable on the max weld induced distortion. The high and low values for each design variable were selected as +/- 33.33% of their baseline value.

Figure 4.11 presents the percentile main effect of each design variable on the max welding induced distortion for four arbitrary welding directions.
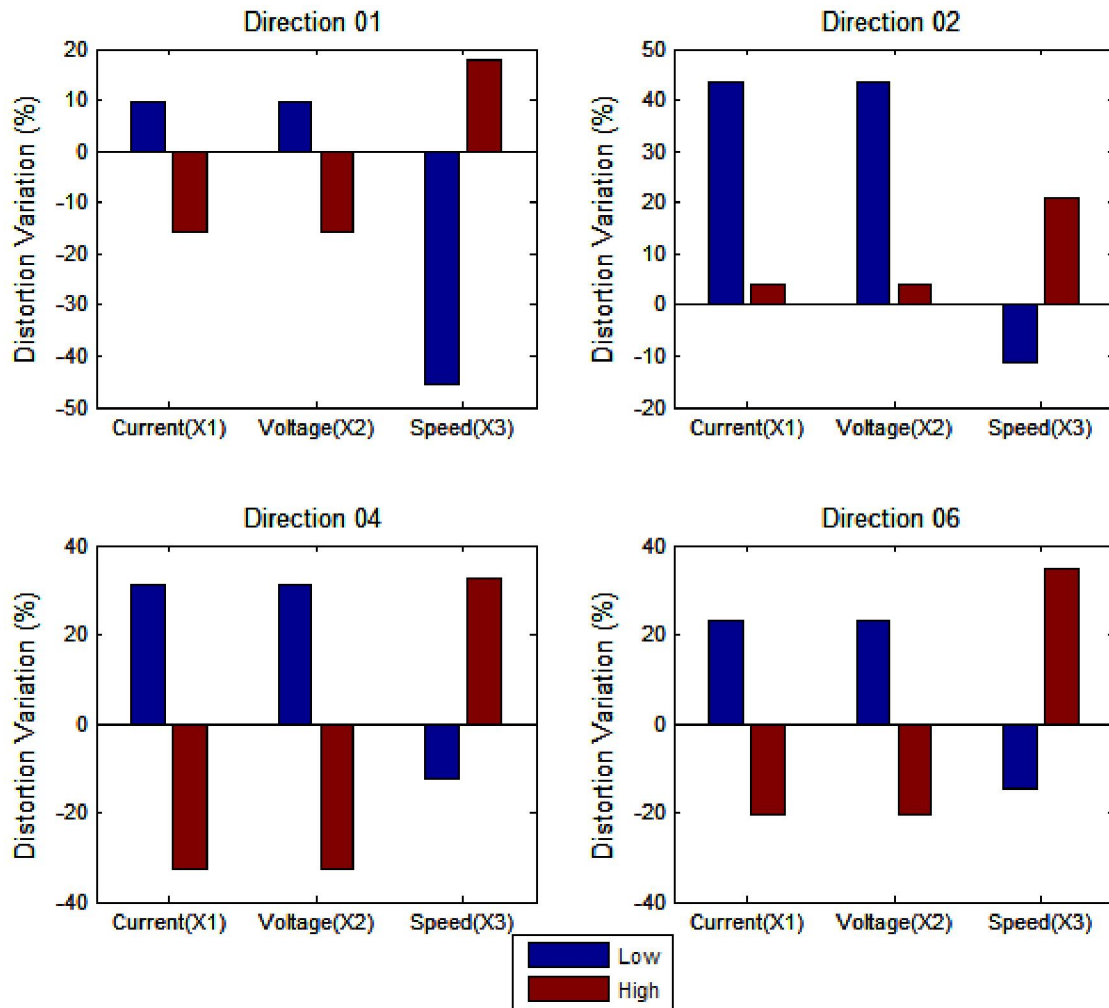
Figure 4.11   Percentile main effects of design variables on max distortion of the lap-joint model

It can be seen through the investigation of the sensitivity results that the main effects of current, voltage and speed on distortion are highly dependent on welding direction for the lap-joint model. For example, current and voltage have less effect on

distortion than welding speed for welding direction 1 but more effect for welding direction 2. For example, decrement of current from baseline value to baseline value -33.33% causes maximum distortion increment of 9.68% and 43.57% for welding direction 1 and welding direction 2 respectively. Increment of voltage from baseline value to baseline value + 33.33% reduces maximum distortion by 15.7% for direction 1 but increases 4.14% for direction 2 and again reduces by 32.43% and 20.63% respectively for welding direction 4 and direction 6.

4.7.2   Direct Computational Optimization Results of Lap-Joint Model

Optimization of the lap-joint model for minimizing the weld-induced distortion was conducted using two different approaches discussed in the previous sections of this chapter. First, the optimization was carried out using direct computational approach. Since GA is not a deterministic algorithm, three trials were conducted to determine the optimum parameters for this case study. The relevant GA parameters used in this approach are shown in Table 4.5.

Table 4.5   GA parameters used in direct computational optimization

Parameter name	Value
Population size	10
No of generations	20
Scaling fitness function	Rank
Parent selection	Stochastic uniform
Elite count	2
Crossover fraction	0.8
Function tolerance	10E-06
Mutation function	Adaptive feasible
Crossover function	Scattered

The optimization results are given in Table 4.6. There is no significant difference in the trials shown. However, the best optimization result is found in trial 2 for the max distortion of 0.422 mm, which is 27.18% less than the max distortion found in the experimental condition (0.58 mm) and 81.55% less than the max distortion in the worst condition (2.29 mm). Furthermore, it is seen that the optimum heat input is 2000 W, which is just 48.78% of the heat input of the experimental condition (4100 W) and 40% of the heat input in the worst condition found during the optimization process. The max distortions found with the other two trials are the same (0.427 mm) and very close to best optimization result. Therefore, GA was successful in determining the optimum set of parameters that would result in the reduced weld induced distortion. A reduced weld speed and heat input together with the weld robot trajectory segmentation into two portions was proven to be effective in reducing weld distortion in this case study.

Table 4.6   Optimization results of direct computational optimization approach

Trial#	Optimum values of design variables				Optimum Distortion, mm	No of Simulations
	X1, Ampere	X2, Volt	X3, mm/s	X4		
1	200	15	10	3	0.427	58
2	200	10	5	3	0.422	63
3	200	15	10	3	0.427	78

Given the high computational expenses, the aim is to optimize the process with a maximum of 100 FE simulations. For all three trials, the optimization converged with 10 to 15 iterations and at the maximum cost of 78 FE simulations in trial 3. The fastest convergence was achieved in trial 1 with 58 FE simulations. In trial 2, the optimum result was achieved with 63 FE simulations. For all the case studies, the optimum point was

reached within 5 or 6 iterations. But the optimization algorithm was designed to run extra five iterations to confirm the validity of the optimum point. Thus, for all three trials, the optimization algorithm stops searching for optimum point when cumulative change in objective function value is less than the predefined limit (10E-06) for five consecutive generations. Figure 4.12 shows the optimization result convergence history with respect to the calculation generations or iterations for trial 2. The convergence history also reveals that the z-directional or out-of-plane distortion is the dominant part of total distortion and it is the most sensitive distortion component to the change in design variables considered.
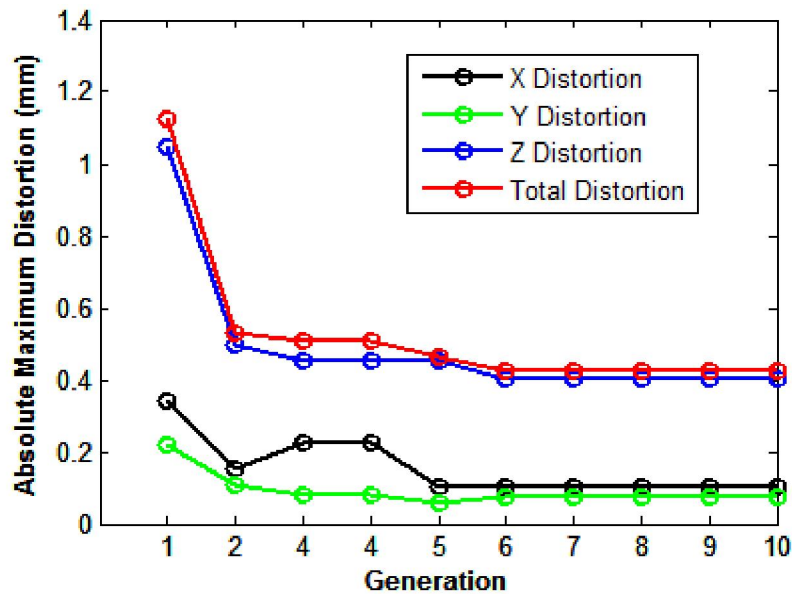
Figure 4.12   Result convergence history for direct computational optimization approach

Next, different welding characteristics of the lap-joint model for optimum set of parameters was investigated by contour plots. Figure 4.13 shows a comparison of weld

74

pool shapes for the experimental, worst and optimum set of parameters. As illustrated in

Figure 4.13, molten zone is almost penetrating through the thickness of the plate since

heat input in the worst condition was almost two times the optimum welding condition.

Also, both the depth of penetration and the heat-affected zone of the experimental

condition are much higher than those of the optimum condition. A too high weld

penetration and heat-affected zone are not desirable as they have adverse effect on the

ultimate performance of the welded structure. Over-welding often increases weld

shrinkage and causes greater distortion. Therefore, optimization of welding parameters is

effective to ensure just adequate welding quality.
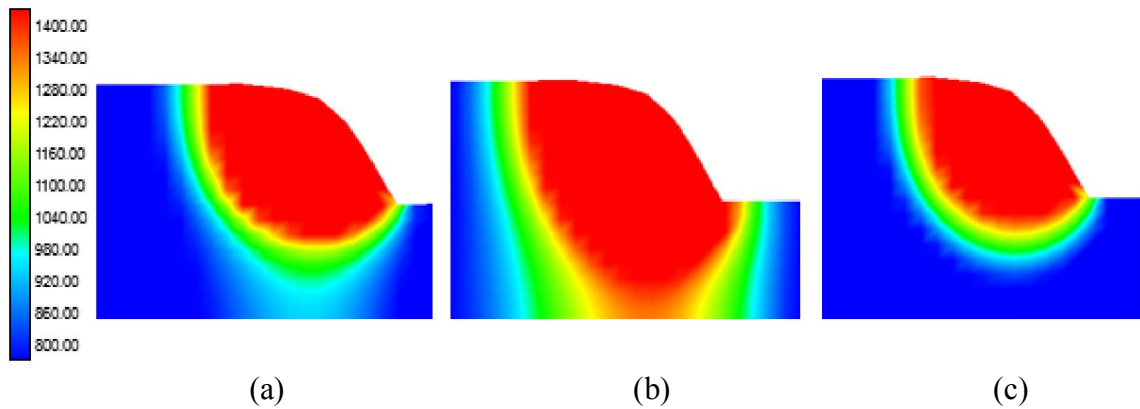
Figure 4.13   Weld pool shape comparison for different conditions by temperature (^{o}C) - (a) experimental condition , (b) worst condition and (c) optimum condition

The total distortion patterns obtained by different welding conditions are shown in

Figure 4.14. It is observed that implementation of optimized welding parameters not only

reduced the maximum distortion but also reduced significantly the overall distortion of

the entire structure. For the optimum condition, distortion of a large area over the surface

of the model is in the order of 0.2 mm or less. As such, optimization of welding

parameters is also effective to reduce the overall weld induced distortion.
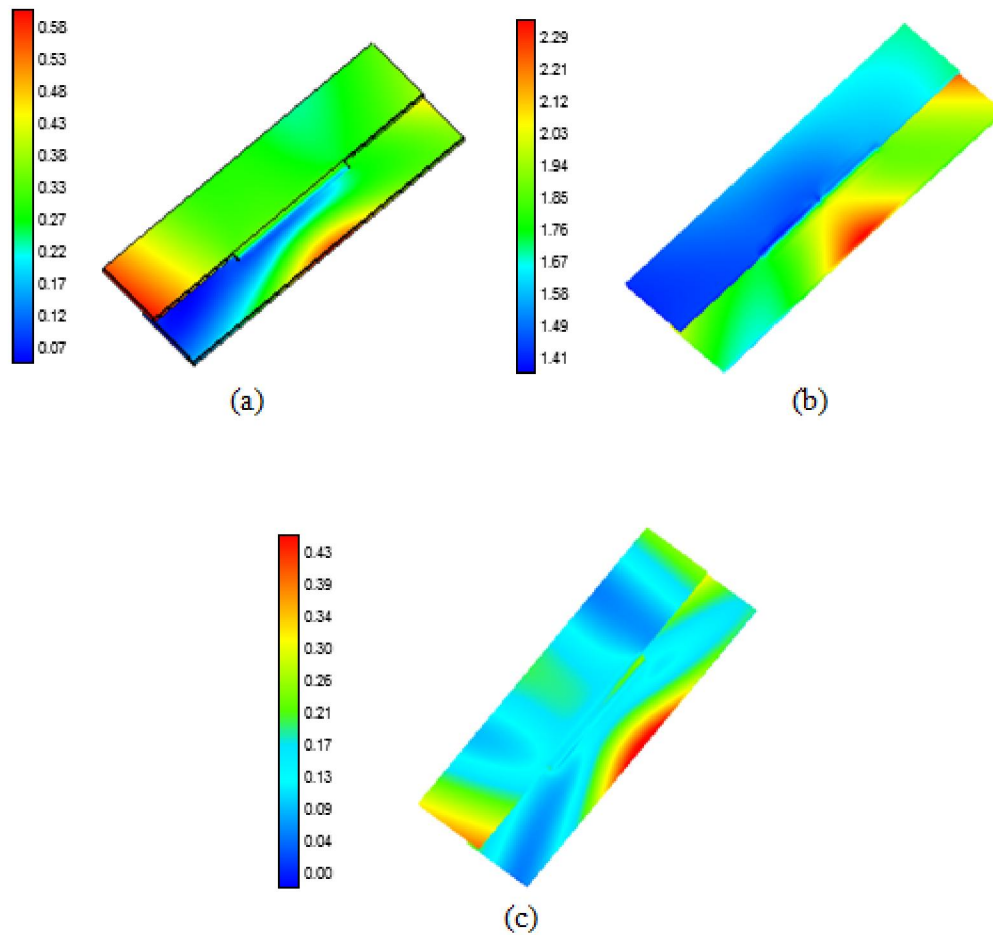
Figure 4.14   Total distortion (mm) pattern comparison for different conditions-
(a) Experimental condition , (b) Worst condition and (c) optimum condition

Since the distortion plots give more quantitative information, distortion along two

edges of the plates were investigated to understand the optimization effect in more detail.

Figure 4.15 illustrates the relevant distortion plots for experimental, worst and optimum

conditions. As shown in Figure 4.15 (a) the distortion distribution along the edge of upper

plate for optimized condition is much more uniform than distortion distribution in

experimental and worst condition cases. For the lower plate, the distortion distribution is
not as uniform as upper plate but the overall distribution is also lower than experimental
and worst condition cases.
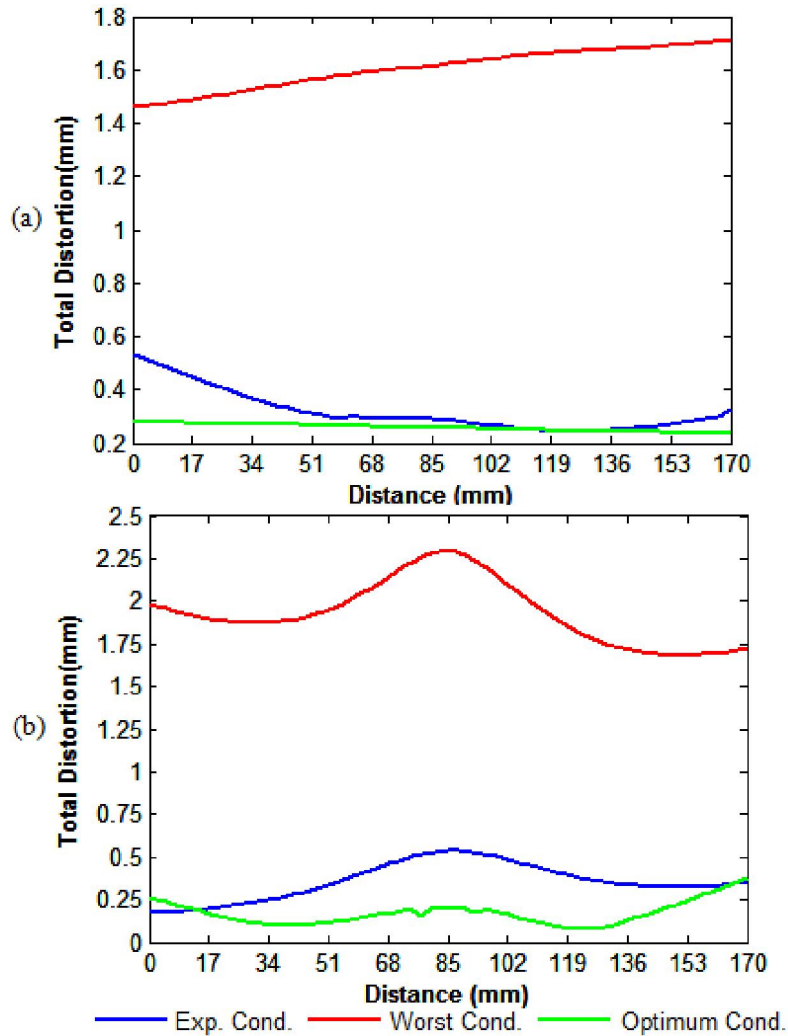
Figure 4.15   Total distortion plots along the edges of the plates for different conditions-
(a) upper plate and (b) lower plate

4.7.3   RSM based Optimization Results of Lap Joint Model

In this approach, a full quadratic PRS model was generated to replace the FE simulation for distortion evaluation during design optimization. Experimental design was created based on a three-level Box-Behnken method with 75 data points. Welding current ranged between 100 and 250 Ampere , arc voltage (10 – 25 Volt) , welding speed (3.5 – 10 mm/s) and six welding directions were applied as design variables. Similar to the sensitivity analysis, a separate DOE table with three design variables was constructed for each welding direction and subsequently, all DOE tables were merged to formulate the final DOE table for all four variables including the welding direction. Table 4.7 shows the experimental design labels of considered variables.

Table 4.7   Experimental design labels of considered variables of lap joint model

Design Variable	S	-1	0	1
Current (Ampere)	X	100	150	250
Voltage (Volt)	X	10	15	25
Welding Speed	X	3.5	7	10

** detailed DOE table is presented in Appendix B.

A second degree polynomial was fitted to the experimental data and the adequacy of the fitted PRS was measured by three different error statistics (i.e., average error, maximum error and root mean square (RMS) error). A trial-error-modification loop based methodology was adopted to improve the fitting of the PRS to the experimental data until the absolute maximum error was 5% or less. It took six trials to reduce the maximum fitting error below 5% as shown in Table 4.8.

78

Table 4.8   Absolute error analysis results of distortion PRS

Trial #	Average Error(%)	Maximum Error (%)	RMS Error (%)
1	3.19	10.64	4.52
2	2.49	9.4	3.48
3	2.23	6.94	3.11
4	1.92	6.16	2.69
5	1.76	5.39	2.46
6	1.74	4.36	2.34

Figure 4.16 shows the relationship between actual and PRS predicted max distortion values. It is evident from the figure that the model is sufficiently accurate as the predictions are placed within acceptable tolerance limit from the diagonal line of actual value.
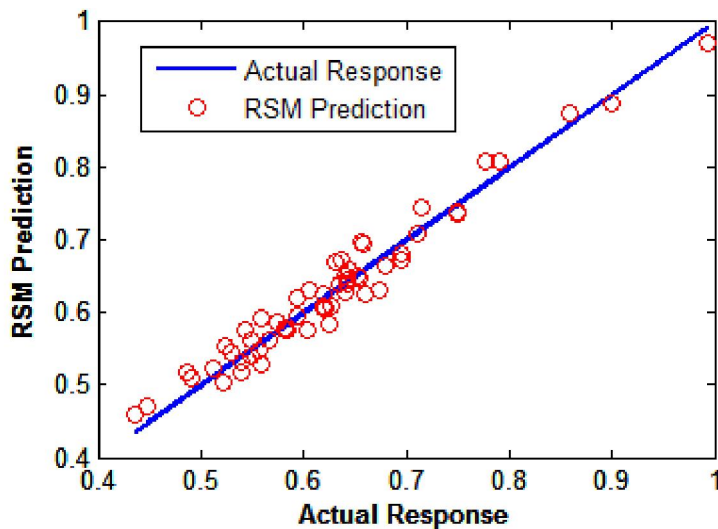
Figure 4.16   Fitness plot of distortion PRS of the lap-joint model

Similarly, a full quadratic response surface model was generated to replace the computation intensive FE simulation during optimization for temperature constraint

79

evaluation. Since temperature constraint is independent of welding direction, only welding current, arc voltage and speed are considered as design variables. Experimental design was created based on a three-level Box-Behnken method with 15 data points and experimental design levels were the same as that shown in Table 4.4. A second degree polynomial was fitted to the experimental data and the PRS with adequate fitting accuracy was obtained with just one trial. Different errors associated with the PRS fitting and resultant fitness plot are shown in Table 4.7 and Figure 4.17, respectively. As shown in Figure 4.17, a temperature constraint value of 1 indicates that the constraint is satisfied.

Table 4.9   Absolute error analysis results of temperature constraint PRS

Trial #	Average Error(%)	Maximum Error (%)	RMS Error (%)
1	0.79	1.83	1.93
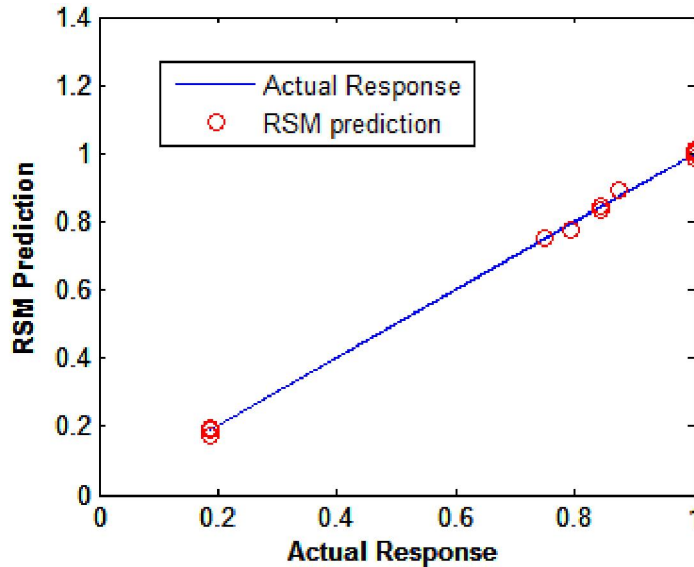
Figure 4.17   Fitness plot of temperature constraint RSM of lap joint model

After building the response surface models for distortion and temperature constraint evaluation, both models were linked with GA solver for welding optimization. The optimization results are illustrated in Table 4.3. Similar to the previous approach, three trials were conducted to determine the optimum parameters for this case study. However, since the objective function and temperature constraint evaluations are much cheaper with the PRS models, a large population size was considered in this approach. The relevant GA parameters used in this approach are shown in Table 4.8.

Table 4.10   Genetic Algorithms parameters used in RSM based optimization

Parameter name	Value
Population size	20
No of generations	20
Scaling fitness function	Rank
Parent selection	Stochastic uniform
Elite count	2
Crossover fraction	0.8
Function tolerance	10E-06
Mutation function	Adaptive feasible
Crossover function	Scattered

The optimization results are illustrated in Table 4.9. All the trials converged to the same optimal point and the max distortion predicted by PRS was 0.453 mm whereas the corresponding simulation prediction was 0.486 mm.

Table 4.11 Optimization results of RSM based optimization approach

Trial #	Optimum values of design variables				RSM-Based Optimum Distortion, mm	Simulation-Based Optimum Distortion, mm	Error (%)
	X1, Ampere	X2, Volt	X3, mm/s	X4			
1	150	20	10	1	0.453	0.486	6.8
2	150	20	10	1	0.453	0.486	6.8
3	150	20	10	1	0.453	0.486	6.8

Figure 4.18 shows the optimization result convergence history with respect to the calculation generations or iterations for trial 1. The convergence history reveals that convergence was achieved with 15 generations for trial 1. Although RSM predicted optimum result is not exactly equal to that of direct optimization approach, it is evident from the results that the RSM results are within acceptable tolerance and practical.
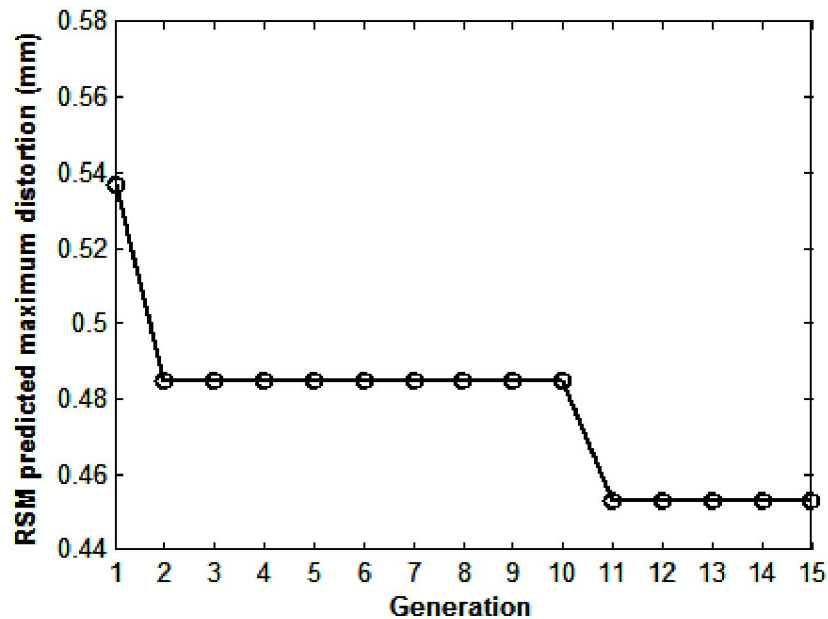
Figure 4.18 Result convergence history for RSM based optimization approach

4.7.4   Direct Computational Optimization Results of Lower-Arm Model

Optimization of the lower-arm model for minimizing weld induced distortion was conducted using direct computational approach only. In this case study, welding path was treated as free design variable, that is, it can take any possible value from the available combinations of three sub-weld order and direction. For three welding orders and two directions for each sub-weld, total possible combinations for welding path are 48 (2^3x 3!). Therefore, it will be difficult and computationally inefficient to implement metamodel based optimization approach considering the number of simulations required to construct a reliable DOE table for metamodel. For example, to build a response surface model with adequate accuracy just like previous case study, minimum number of simulations required is 480 considering at least 10 data points for each of the 48 directions. Considering the difficulty of implementing metamodel-based approach, an effort was made to investigate this case study with direct computational optimization approach. Given the high computational expense, the aim is not to find the best possible result but to evaluate how much distortion can be reduced through the optimization process with a maximum of 100 FE simulations. Same GA parameters of the previous case with a population size of 10 and 10 generation were used.

The optimization results are illustrated in Table 4.12. The best result or smallest distortion found for this case study is 0.35 mm, which is 53.33% less than the worst result or largest distortion (0.75 mm). Furthermore, it is seen that heat input for the best parameter set is 2870 W, which is 18.6% less than the heat input (3525 W) of the worst parameter set. Figure 4.19 illustrates the best and worst welding sequence found for this

83

case study. So, it is also possible to reduce the weld-induced distortion considerablely by GA at the cost of 100 FE simulations.

Table 4.12   Optimization results of lower-arm model

	Optimum value of design variables						Distortion
	X1, Ampere	X2, Volt	X3, mm/s	X4	X5	X6	Value, (mm)
Best	140	20.5	22	6	4	2	0.35
Worst	150	23.5	18	1	6	5	0.75
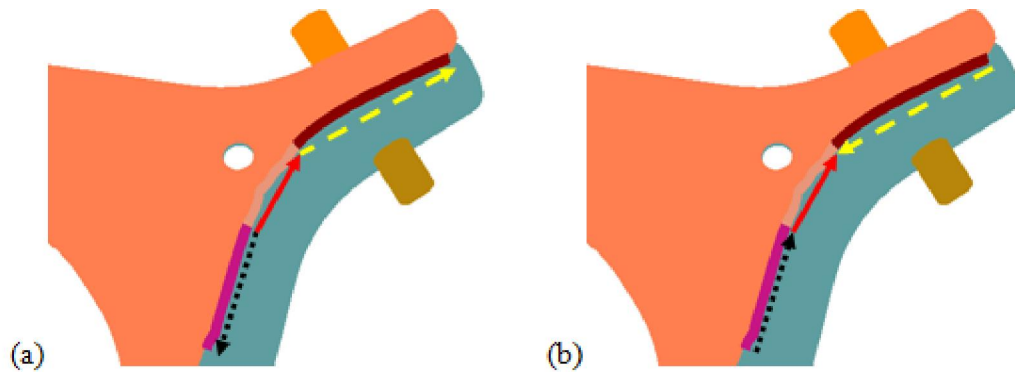
Figure 4.19   Illustration of the best and worst welding sequence found in this study- (a) best weld sequence and (b) worst weld sequence

CHAPTER V

CONCLUSION AND FUTURE WORK

Over the past decade, a tremendous growth has been observed in the use of CAE tools in manufacturing process design and analysis. By using CAE tools for numerical simulation of manufacturing processes, it is possible to predict the quality of finished product and identify potential defects during early design phase. Since a computer simulation is faster and cheaper than performing a real test, it reduces manufacturing cost and the time-to-market. Design optimization always requires a loop of design-evaluate-redesign. Therefore, the ability to quickly and easily assess desired process dependent responses accelerates the ultimate process of optimum design. Furthermore, selecting appropriate optimization methodology also reduces the required number of costly simulation runs as well as increases the fidelity of the optimization process. Hence, automated design optimization of welding process based on integrated CAE tools can contribute substantially to enhance final welded product, to facilitate and accelerate the product design and development.

This study introduces a robust computational optimization system based on integrated CAE tools which allows automatic optimization of welding process parameters without the requirement of expensive real experiments. The system is capable of exploring the effect of several design variables at a time with limited modification in

simulation model. Thereby, the developed tool can be effectively implemented for the optimum design of a large scale industrial welding process.

The illustrative example of lap joint welding specimen optimization presented in this work shows that the proposed GA-FEM coupled method is able to search for optimum set of process parameters specially under the critical constraint of weld quality requirement. In this optimization problem, an straightforward solution approach is to run all possible 368 (4x4x4x6) combinations and select the best one as optimum solution. However, it will be computationally inefficient and sometimes infeasible considering the extensive computational time required for FE simulation. Using GA, we achieved optimum results with maximum 78 FE simulations. So, the method is certainly effective for this case study. Moreover, meta-model based optimization technique using response surface methodology has also been implemented to replace computation intensive FE simulations. In order to treat discrete design variable like welding path, a modified DOE table has been constructed to fit RSM. The optimization results of this approach was also close to that of direct approach.

To examine the maturity of the developed system, a realistic automotive structure with nonlinear weld path has been investigated in next stage. In absence of any prior work, numerical or experimental, simulation model has been calibrated based on author's experience only. For this case study, six design variables have been selected including welding sequence of three sub-welds. Total combination for this study is 3072 ($4x4x4x2^3x3!$). Only direct computational optimization approach was applied to this case study. The estimated computational cost of building an adequate RSM for this model is approximately 480 FE simulations. As such, as a trade off, direct computational approach

with a restriction of maximum 100 FE simulations was implemented. the best result found by GA within this limit was 53.33% less than the worst result encountered during optimization process. This example illustrates that the proposed computational system can be redesigned easily without any major modification in system when the objective is to find a compromise or trade-off between optimum design and computational cost. The direct computational method is also superior to meta-model based technique in terms of problem dependency. One major drawback of meta-model based approach is that there is no general method to develop a meta-model for a specific problem. One meta-model might work properly in some cases but not for all cases. Therefore, necessity of generating a separate meta-model for different cases increases substantially the size of the DOE matrix which ultimately results in large computational cost.

Although computational efficiency is a critical limitation of the proposed GA-FEM coupled optimization system, it is evident that the methodology is quite successful in converging towards optimum point. To increase the computational efficiency of the developed system, integration of parallel computing facility with the system can be an excellent extension of current work. Consideration of additional design variables such as clamping position, clamp apply/release time and cooling time between sub-welds will also be the objects for future research in this arena. Furthermore, there is also a great scope of studying more versatile meta-modeling techniques that can handle welding path or sequences more efficiently to replace computation intensive welding simulations.

REFERENCES

[1]   Michaleris, P., Minimization of Welding Distortion and Buckling, Woodhead Publishing, 2011, pp. 3.

[2]   Tsai, C. L., Park, S. C. and Cheng, W. T., "Welding Distortion of This-Plate Panel Structure," Welding Research Supplement, 1999, pp. 156-164.

[3]   Connor, P. Leonard, Welding Handbook : Welding Technology, American Welding Society, Volume 1, eighth edition, pp. 4, 1987.

[4]   Kou, Sindo, Welding Metallurgy, John Wiley & Sons,Inc, second edition, pp. 13, 2003.

[5]   http://www.lincolnelectric.com/en-us/support/welding-how-to/Pages/weld-distortion-detail.aspx

[6]   Masubhichi, Koichi, Analysis of welded structures , Pregamon Press, 1980.

[7]   Feng, Zhili, Processes and mechanisms of welding residual stress and distortion, Woodhead Publishing and Maney Publishing, pp. 228, 2005.

[8]   Goldak, J. A., and Akhlagi, M., Computational Welding Mechanics, Springer, New York, pp. 79, Chap. 3, 2005.

[9]   Y. Ueda and T. Yamakawa, Analysis of thermal elastic-plastic stress and strain during welding by finite element method, JWRI, vol. 2, no. 2, pp. 90-100, 1971.

[10]   H. D. Hibbitt and P. V. Marcal, A Numerical Thermo-Mechanical Model for the Welding and Subsequent Loading of a Fabricated Structure, Computers & Structures, vol. 3, pp. 1145-1174, 1973.

[11]   Lindgren, Lark-Erik, Computational Welding Mechanics, Springer, Woodhead Publishing and Maney Publishing, pp. 3, 2007.

[12]   Lindgren, L.-E., "Finite Element Modeling and Simulation of Welding, Part 1: Increased Complexity," Journal of Thermal Stresses, 24, pp. 141-192, 2001.

[13]   Lindgren, L.-E., "Finite Element Modeling and Simulation of Welding, Part 2: Improved Material Modeling," Journal of Thermal Stresses, 24, pp. 195-231, 2001.

[14] Lindgren, L.-E., "Finite Element Modeling and Simulation of Welding, Part 3: Efficiency and Integration," Journal of Thermal Stresses, 24, pp. 305-334, 2001.

[15] B. A. B. Andersson, Thermal Stresses in a Submerged-Arc Welded Joint Considering Phase Transformations, ASME J. Engineering Materials and Technology, vol. 100, pp. 356-362, 1978.

[16] E. F., Rybicki, D. W., Schmueser, R. B., Stonesifer, J. J., Groom and H. W. Mishler; J. Pressure Vessel Technol., 100, pp. 258-262, 1978.

[17] Brickstad, B., Josefon, B., L., A Parameteric Study of Residual Stresses in Multi-pass Butt Welded Stainless Steel Pipies, International Journal of Pressure Vessel & Piping, 75,pp. 11-12,1998.

[18] Brown, S., and Song, H., Finite element simulation of welding of large structures, ASME Journal of Engineering for Industry, 114, (4), 441-451, 1992.

[19] Y. Fujita, T. Nomoto and H. Hasegawa, Thermal stress analysis based on initial strain method, 1979, IIW Doc X-926-79.

[20] E. F. Rybicki and R. B. Stonesifer, An analysis for predicting weld repair residual stresses in thick-walled vessels, ASME J. Pressure Vessel Technology, vol. 192, August, 1980, pp. 323-331.

[21] P. Michaleris and A. Debiccari, A Predictive Technique for Buckling Analysis of Thin Section Panels due to Welding, Journal of Ship Production, 12(4), pp. 269-275, 1996.

[22] P. Michaleris and A. DeBiccari, Prediction of welding distortion, Welding Journal, vol. 76, no 4, 1997, pp. 172s-181s.

[23] P. Tekriwal. And J. Mazumder, Transient and residual thermal strain-stress analysis of GMAW, ASME J. Engineering Materials and Technology, vol. 113, pp. 336-343, 1991.

[24] Karlsson, R. I., and Josefson, B.L., Three-dimensional finite element analysis of temperature and stresses in a single-pass butt welded pipe. 1988.

[25] Mahin, K. W, Shapiro, A., B., and Hallquist, J., Assessment of boundary condition limitations on the development of a general computer model for fusion welding. International Conference on Trends in Welding Research, Gatlinburg, Tenn., 1986.

[26] Goldak, J., Oddy, A., McDill, M., and Chakravarti, A., Progress in computing residual stress and strain in welds. International Conference on Trends in Welding Research, Gatlinburg, Tenn., 1986.

[27] Ueda, Y., and Murakawa, H., Applications of computer and numerical analysis techniques in welding research. Transactions of JWR113(2) :165-1 74, 1984.

[28] Michaleris, P., , Minimization of Welding Distortion and Buckling, Woodhead Publishing, 2011, pp. 17.

[29] Rosenthal D.: the theory of moving sources of heat and its application to metal treatments, Trans ASME, Vol. 68, p 849-865, 1946.

[30] Nguyen, N. T., Ohta, A., Matsuoka, K., Suzuki, N, and Maeda, Y., Analytical Solutions for Transient Temperature of Semi-Infinite Body Subjected to 3-D Moving Heat Sources, Welding Research Supplement, 265-s, 1999.

[31] Pavelic V., Tanbakuchi R.,   Uyehara   0. A.   and Myers: Experimental and computed temperature histories in gas tungsten arc welding of thin plates, Welding Journal Research Supplement, Vol. 48. pp 295s-305s, 1969.

[32] Friedman, E., Thermo-mechanical analysis of the welding process using the finite element method, Journal Pressure Vessel Technology, Trans. ASME, Vol. 97, NO 3, pp 206-213, 1975.

[33] Andersson, B.A.B., Thermal stresses in submerged-arc welded joint considering phase transformation, Journal of Engineering Materials and Technology, Trans. ASME, Vol. 100, pp 356-362, 1978.

[34] Goldak, J., Chakravarti, A. and Bibby, M., A New Finite Element Model for Welding Heat Sources, Metallurgical Transactions B, 15B, pp. 299-305, 1984.

[35] Radaj, Dieter, Welding Residual Stresses and Distortion, Verlag für Schweissen und Verwandte Verfahren, DVS-Verlag, 2003.

[36] Feng, Zhili, Processes and mechanisms of welding residual stress and distortion, Woodhead Publishing and Maney Publishing, pp. 3, 2005.

[37] Daniewicz, S. R., McAninch, M. D., McFarland, B., and Knoll, D., Application of distortion control technology during fabrication of large offshore structures. Proc. of AWS/ORNL International Conference on Modeling and Control of Joining Processes, 1993.

[38] Murakawa, H., Luo, Y., Ueda, Y., Prediction of welding deformation and residual stress by elastic FEM based on inherent strain (1st report)- mechanism of inherent straint production, J. Soc. Nav. Architects Jpn., 180, pp. 739-751, 1996.

[39] Luo, Y., Murakawa, H., Ueda, Y., Prediction of welding deformation and residual stress by elastic FEM based on inherent strain (2nd report)- deformation and residual stress under multiple thermal cycles, J. Soc. Nav. Architects Jpn. 182, pp. 783-793, 1997.

[40] Hinrichsen, B, Prediction of welding induced distortion in ship structures, Ship Technol. Res. 46, pp. 153-63, 1999.

[41] Teng, Tso-Liang, Fung, Chin-Ping, Chang, Peng-Hsiang, Yang, Wei-Chun, Analysis of residual stresses and distortions in T-joint fillet welds, International Journal of Pressure Vessels and Piping 78, pp. 523-538, 2001.

[42] Jung, H., Tsai, C.L., Plasticity-based distortion analysis for fillet welded thin-plate T-joints. Weld. J. 83 (6), pp. 177-187, 2004.

[43] Camilleri, D, Gray, T G F, Computationally efficient welding distortion simulation techniques, Modeling Simul. Mater. Sci. Eng. 13, pp. 1365-1382, 2005.

[44] Deng, Dean, Murakawa, Hidekazu, Prediction of welding distortion and residual stress in a thin plate butt-welded joint, Computational Materials Science 43 , pp. 353-365, 2008.

[45] Deng, Dean, Liang, Wei, Murakawa, Hidekazu, Determination of welding deformation in fillet welded joint by means of numerical simulation and comparison with experimental measurements, Journal of Materials Processing Technology, 183, pp. 219-225, 2007.

[46] Deng, Dean, Murakawa, Hidekazu, Liang, Wei, Numerical Simulation of welding distortion in large structures, Computer Methods Appl. Mech. Engrg., 196, pp. 4613-4627, 2007.

[47] Deng, Dean, Murakawa, Hidekazu, and Liang, Wei, Prediction of welding distortion in a curved plate structure by means of elastic finite element method, Journal of Materials Processing Technology, 203, pp. 252-266, 2008.

[48] Deng, Dean, Murakawa, Hidekazu, and Ninshu, Ma, Prediction of welding deformation in thin plate panel structure by means of inherent strain and interface element, Science and Technology of Welding & Amp Joining, Vol. 17, Issue 1, pp. 13-21, 2012.

[49] Benyounis, K. Y., and Olabi, A. G., Optimization of different welding processes using statistical and numerical approaches- A reference guide, Advances in Engineering Software, 39, pp. 483-496, 2008.

[50] J Dhas, Edwin Raja, and S Dhas, Jenkins Hexley, A review on optimization of welding process, Procedia Engineering, 38, pp.. 544-554, 2012.

[51] Feng, Zhili, Processes and mechanisms of welding residual stress and distortion, Woodhead Publishing and Maney Publishing, pp. 270, 2005.

[52] J. E. V. Petera, and R. P. Dwight, Numerical Sensitivity Analysis for Aerodynamic Optimization : A Survey of Approaches, Computers & Fluids 39, pp. 373-391, 2010.

[53] Asadi, Mahyar, and Goldak, John A., A Framework for Designer-Driven Exploration of Computational Weld Mechanics Design Space, PVP2011-57917, Proceedings of the ASME 2011 Pressure Vessels & Piping Division Conference, Maryland, USA, 2011.

[54] P. Michaleris, D. A. Tortorelli, and C. A. Vidal, Analysis and Optimization of Weakly Coupled Thermo-Elasto-Plastic Systems with Applications to Weldment Design, International Journal for Numerical Methods in Engineering, 38, pp. 1259-1285, 1995.

[55] P. Michaleris, J. Dantzig, and D. A. Tortorelli, Minimization of welding residual stress and distortion in large structures.

[56] Song, J., Peters, J., Noor, A., P. Michaleris, Sensitivity analysis of the thermomechanical response of welded joints, International Journal of Solids and Structures, 40, pp. 4167-4180, 2003.

[57] Kadivar, M. H., Jafarpur, K., and Baradara, G. H., Optimizing welding sequence with genetic algorithm, Computational Mechanics, 26, pp. 514-519, 2000.

[58] Voutchkov, I., Keane, A. J., Bhaskar, A., and Olsen, M. Tor, Weld sequence optimization : The use of surrogate models for solving sequential combinatorial problems, Comput. MethodsAppl. Mech. Engrg., 194, pp. 3535-3551, 2005.

[59] Asadi, Mahyar and Goldak, John A., Combinatorial optimization of weld sequence by using a surrogate model to mitigate a weld distortion, Int. J Mech Mater Des, 7, pp. 123-139, 2011.

[60] Goldak, J. and Asadi, M., "Computational Weld Mechanics and Optimization of Welding Procedures, Welds and Welded Structures," *Transactions of JWRI, Special Issue on WSE2011*, Osaka, Japan, pp. 55-60, 2011.

[61] Lewis, R., P. Nithiarasu, and K. Seetharamu, Fundamentals of the Finite Element Method for Heat Transfer and Fluid Flow, Jon Wiley & Sons., 2004.

[62] Carlsaw, H. and J. Jaeger, Conduction of Heat in Solids, Clarendon Press, 2nd edn, 1959.

[63] http://www.simufact.de/en/solutions/sol_weld.html.

[64] simufact.welding 3.1 manual , 2012.

[65] Rais-Rohani, Masoud, Engineering Design Optimization Course Lecture, Mississippi State University, 2012.

[66] Park, Hong-Seok and Dang, Xuan-Phuong, Structural optimization based on CAD-CAE integration and metamodeling techniques, Computer Aided Design, 42, pp. 889-902, 2010.

[67] Goldberg, D. E., Genetic Algorithms in Search, Optimization & Machine Learning, Addison-Wesley, Massachusetts, Chap. 1, 1989.

[68] Montgomery, D.C., Design and Analysis of Experiments, Fourth Edition. New York: John Wiley & Sons, 1997.

[69] http://www.mathworks.com/products/global-optimization/description4.html

APPENDIX A

WELDING EXPERIMENTS FOR LAP-JOINT MODEL

A.1   Experimental Setup

Experiments were carried out for the single pass welded lap joint specimen. The plate dimensions are 170mm by 35 mm by 3.2 mm and the weld length is 70 mm at the middle section of the plates. Before welding, the plates were held in position tightly together by using four spring clamps to prevent movement or separation during welding. The experiment setup with necessary dimensions has been shown in Figure A-1.

(a)   (b)
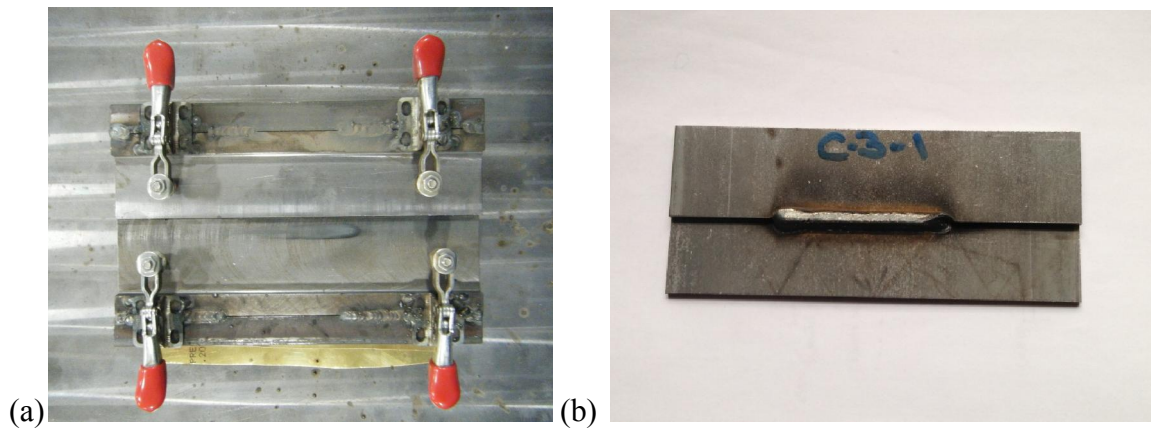
Figure A.1   Experimental model description-

(a) Experimental Setup for lap joint specimen and (b) lap welded sample

The experiments was carried out for parameters given in Table A-1.

Table A.1   Experimental Welding Input Parameters

Set No.	Speed (mm/s)	Current (A)	Voltage (V)	Heat Input (W)	Fixture Release Time (s)
1	10	200	20.5	4100	20

The welding operation was carried out using an industrial welding robot MOTOMAN-UP20(YASUKAWA). The robot had a rotatable table for supporting the

specimens and keeping the weld line parallel to the ground level constantly. The welding

gun was held by the robot, and aside from desired welding directions it could maintain

both up and down, stand-off distance, and angular movements . A welding gun leading

angle of 10 degrees, included angle of 60 degrees and stick out of 12 mm was used in the

experiments to provide an adequate protection of the weld pool. Gas mixture of 80%

argon and 20% of CO2 at a constant flow rate of 18 l/min was used for shielding. The

material of the plates is ASTM A591M-89 sheet metal steel. Sheet metal steel solid filler

wire AWS A5.18-2005 of 0.045 inch diameter was used. The chemical composition of

the base metal and weld bead has been shown in Table A-2.

Table A.2   Chemical Composition of base metal and filler metal

Elements	C	Si	Mn	P	S	B	Al	Cr	Mo	Ni	Cu
Base Metal	0.173	.07	.072	.011	.004	.0002	.044	.05	.004	.02	.005
Filler Metal	0.1	.04	.95	.006	.004	-	-	.02	-	.02	.17

A.2   Temperature and Distortion Measurements

During the tests temperature was measured using FLIR –THERMACAMT400

infrared camera. It provides contactless and fast measurement of transient temperature

distribution over the plates. It provides opportunity to visually inspect temperature

distribution over large area at different time intervals and higher temperature regions can

be identified easily (Figure A-2). The temperature was measured in celsius unit. The

camera could capture temperature in the range from 1300°c to 80°c. The time required to

cool down to the lowest temperature bond of 80°c measurable with this device was

around three minutes.
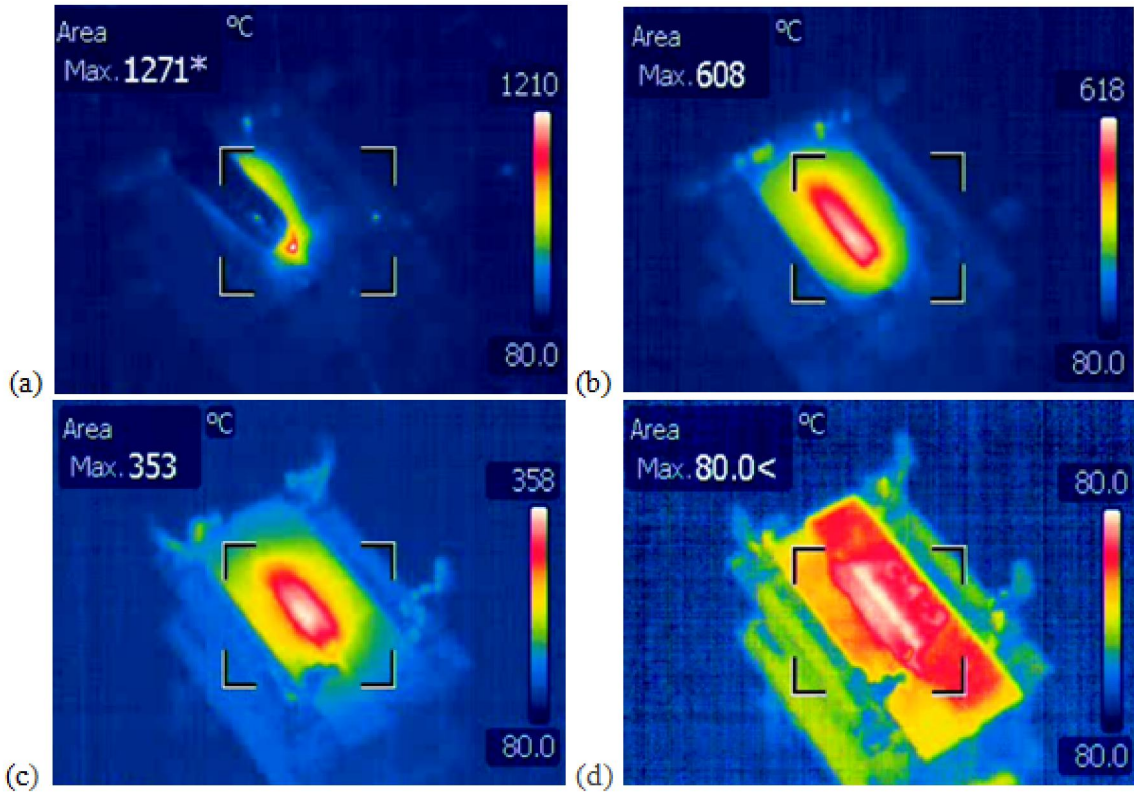
Figure A.2   Temperature measurments at different time intervals using infrared camera-
(a) temperature measurement at 5s, (b) temperature measurement at 12s, (c) temperature
measurement at 20s and (d) temperature measurement at 180s.

Laser ScanArm was used to measure the weld induced distortion in the part. For

distortion calculation, the welded part was compared to a reference object which was just

two plates glued together. The device could only measure out-of-plane distortion. Figure

A-3 shows the distortion pattern obtained after complete cool down. The measurements

were reported in the form of graphical data represented by colored patterns indicating

distortion relative to the pre-welding condition. Distortion has been reported as positive

distortion where the plate has distorted away or out of reference CAD model and it is

recorded as negative distortion where it has distorted inside CAD model.

97
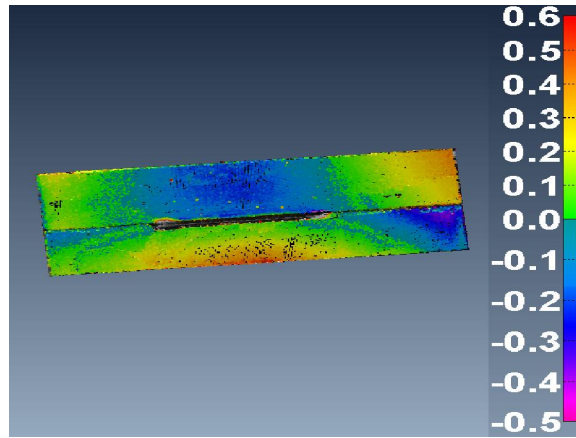
Figure A.3   Distortion patterns for different sets of welding parameters

A.3   Weld Macro Tests

Macro examination is the procedure in which a weld specimen is etched and evaluated macrostructurally at low magnifications. It is a frequently used technique for evaluating weld joint quality characteristics. After welding experiments, the welding macro tests were performed to investigate primarily presence of defects, weld pool shape and depth of weld penetration. The macro samples were prepared by sectioning a test weld, polishing the cut surface smooth and bright and then etching with a suitable reagent. The tests were performed and repeated in three different areas of start, middle and at the end cross section of the samples along the welding path. A macrograph of the weld cross-sectional view of the specimen (at 35mm depth from starting point) is shown in Figure A-4 and corresponding parameters are given in Table A-3.
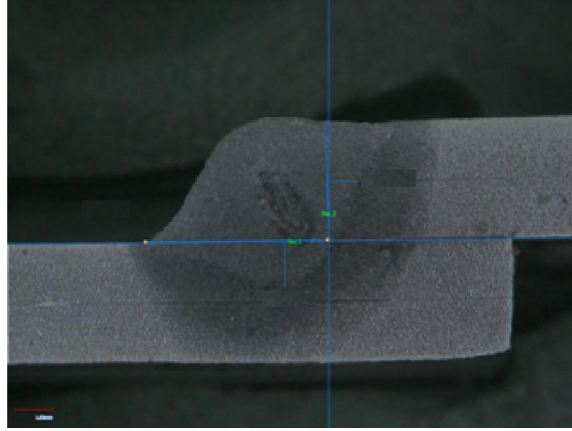
Figure A.4   Typical macrograph of weld cross section

 (35 mm from weld start position)

Table A.3   Weld Macro Test Results (Figure A.4)

	Thickness			Criteria (mm)		Actual Value	% of min	Judgment
Leg Length	2.9	L-A	L1	115% of tmin	3.34	4.84	145.13%	OK
Throat	2.9	T	L3	60% of tmin	1.74	3.17	182.18%	OK
Penatration	2.9	P-A	L4	5% of tmin	0.23	1.23	530.17%	OK
	3.5	P-B	L5	5% of tmin	0.23	0.74	318.97%	OK
Undercut	3.5	U-A	L6	20% of Tmax	0.53	0	0.00%	OK
	3.5	U-B	L7	20% of Tmax	0.53	0	0.00%	OK
tmin value	3.2mm		Tmax value	3.2mm				

The macro test results indicate that all the welds performed during experimental study were free of foreign inclusions or internal defects. Furthermore, all the welds satisfied minimum depth of weld penetration and other dimensional requirements to ensure good weld quality.

APPENDIX B

DOE TABLE FOR RESPONSE SURFACE MODELING OF LAP JOINT MODEL

No.	Current (X1) (Amp)	Voltage(X2) (Volt)	Speed (X3) (mm/s)	Weld Direction(X4)	Distortion (mm)
1	100	25	7	1	0.43574
2	250	15	3.5	1	0.99343
3	150	25	10	1	0.5592
4	150	15	7	1	0.5227
5	150	15	7	1	0.5227
6	250	15	10	1	0.55941
7	250	10	7	2	0.52994
8	200	20.5	5	2	0.89917
9	200	20.5	10	2	0.67397
10	150	15	7	2	0.5124
11	150	15	7	2	0.5124
12	150	15	7	2	0.5124
13	150	20.5	10	2	0.48607
14	200	20.5	10	2	0.67397
15	250	20.5	10	2	0.71502
16	200	25	10	2	0.71163
17	150	20.5	10	2	0.48607
18	200	15	3.5	2	0.77707
19	150	25	5	2	0.78981
20	100	25	7	3	0.49048
21	250	15	10	3	0.62726
22	150	20.5	7	3	0.66021
23	250	15	10	3	0.6187
24	150	15	7	3	0.55591
25	150	15	7	3	0.55591
26	150	15	7	3	0.55591
27	150	25	10	3	0.54263
28	200	20.5	10	3	0.6535
29	200	10	3.5	3	0.63492
30	250	15	10	3	0.62726
31	150	20.5	7	3	0.66021
32	200	20.5	10	3	0.6535
33	100	20.5	5	3	0.52362
34	100	25	7	4	0.54921
35	250	10	7	4	0.54921
36	100	15	3.5	4	0.60451
37	250	15	10	4	0.6187

No.	Current (X1) (Amp)	Voltage(X2) (Volt)	Speed (X3) (mm/s)	Weld Direction(X4)	Distortion (mm)
38	150	25	10	4	0.6187
39	150	15	7	4	0.5841
40	150	15	7	4	0.5841
41	150	15	7	4	0.5841
42	250	25	10	4	0.85809
43	200	10	5	4	0.57417
44	200	15	7	4	0.65302
45	200	15	7	4	0.65318
46	150	15	5	4	0.60548
47	150	25	10	4	0.62149
48	150	15	3.5	4	0.65762
49	100	25	5	4	0.6414
50	100	20.5	5	4	0.62467
51	200	20.5	10	4	0.63107
52	100	25	10	4	0.44866
53	100	25	7	5	0.58244
54	250	10	7	5	0.58244
55	250	15	10	5	0.64314
56	250	10	10	5	0.53921
57	100	25	10	5	0.53921
58	150	25	7	5	0.74885
59	200	10	3.5	5	0.67996
60	150	15	5	5	0.64421
61	150	25	10	5	0.64314
62	200	20.5	10	5	0.65687
63	250	15	10	5	0.64314
64	200	15	7	5	0.63708
65	250	15	7	5	0.74883
66	150	25	7	5	0.74885
67	200	10	3.5	5	0.67996
68	100	25	7	6	0.59375
69	250	10	7	6	0.59375
70	250	15	10	6	0.69527
71	150	25	10	6	0.69527
72	150	15	7	6	0.641
73	150	15	7	6	0.641
74	150	15	7	6	0.641
75	250	10	10	6	0.56622